Microscopía Electrónica de Transmisión: Difracción de Electrones

MT774
Caracterización de Materiales

Alejandro Zúñiga

5 de septiembre de 2007

¿Por qué TEM?

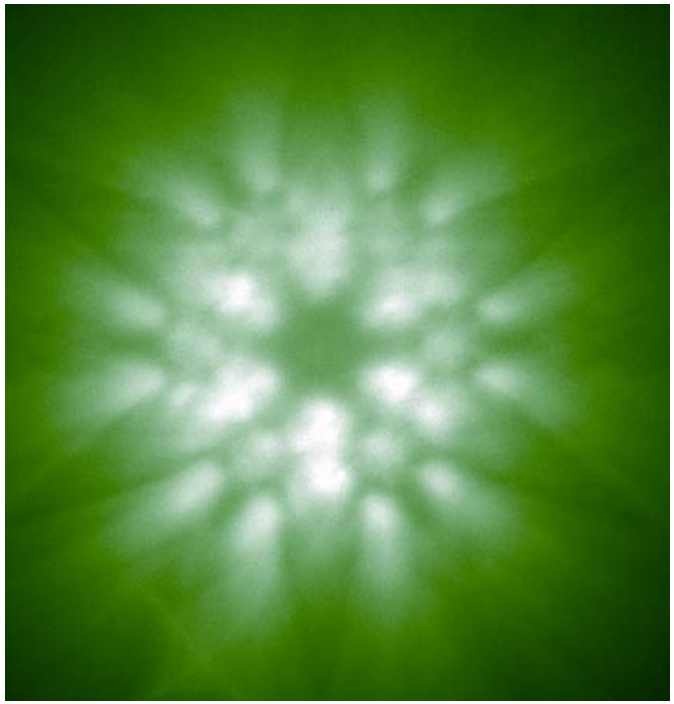

Dispersión de electrones

Resolución → 0.1–0.2 nm

- Resolución (Imágenes)
  - MO: ~ 200 nm
  - SEM: ~ 1 – 3 nm
  - **TEM: 0.1 – 0.2 nm (record de 0.08 nm)**
- Información Cristalográfica
- Composición química (nanoanálisis)
- Y lo mejor … ¡Todo al mismo tiempo!

El Microscopio Electrónico de Transmisión

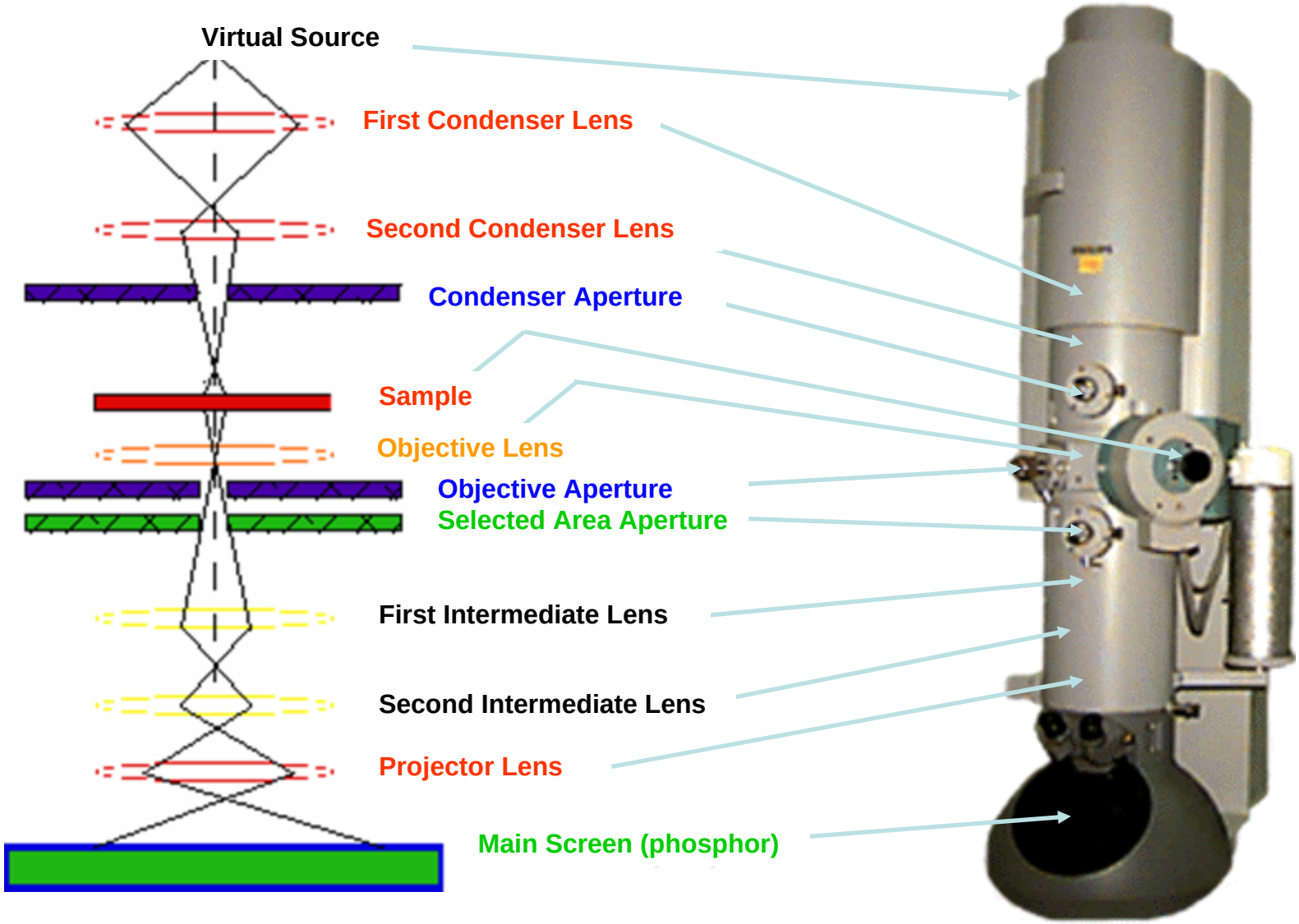

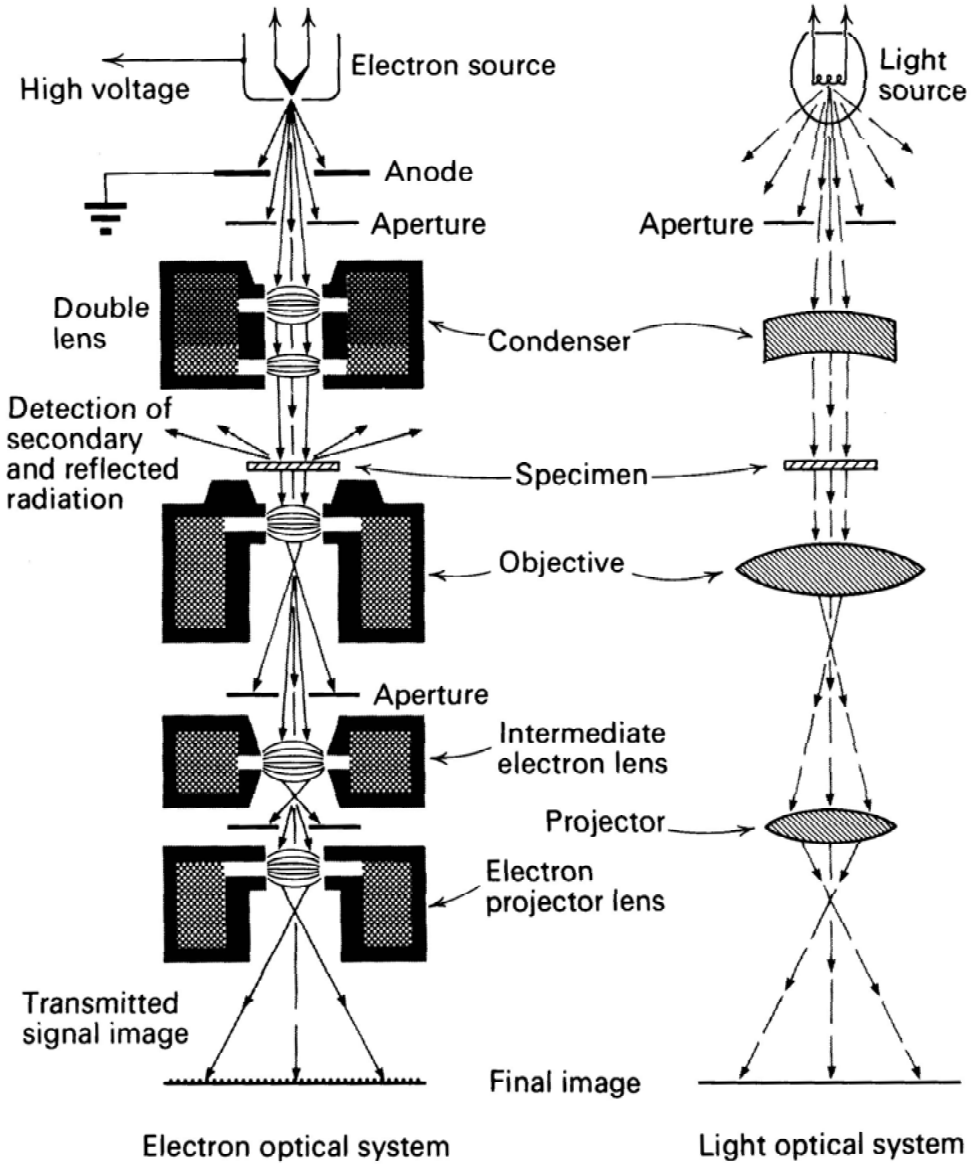

FIG. 3.8 *Schematic comparison of basic light-optical and electron optical microscope systems.*

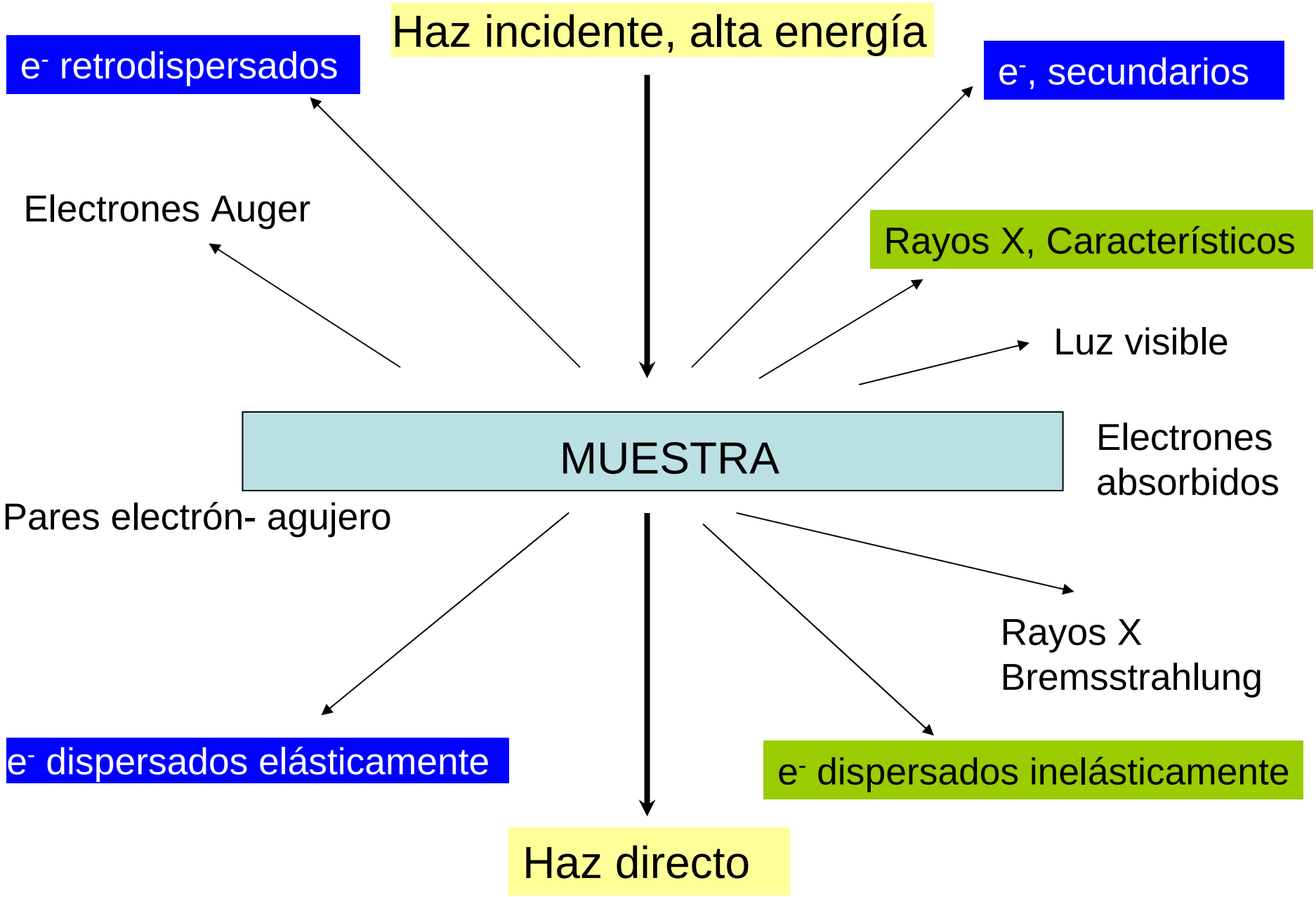
Haz incidente, alta energía
e- retrodispersados
e-, secundarios
Electrones Auger
Rayos X, Característicos
Luz visible
MUESTRA
Electrones absorbidos
Pares electrón- agujero
Rayos X Bremsstrahlung
e- dispersados elásticamente
e- dispersados inelásticamente
Haz directo

A medida que los electrones atraviesan la muestra pueden ser dispersados por una variedad de procesos, o bien no sufrir cambio alguno.

El resultado final es que una distribución no homogénea de electrones emerge desde la superficie inferior de la muestra.

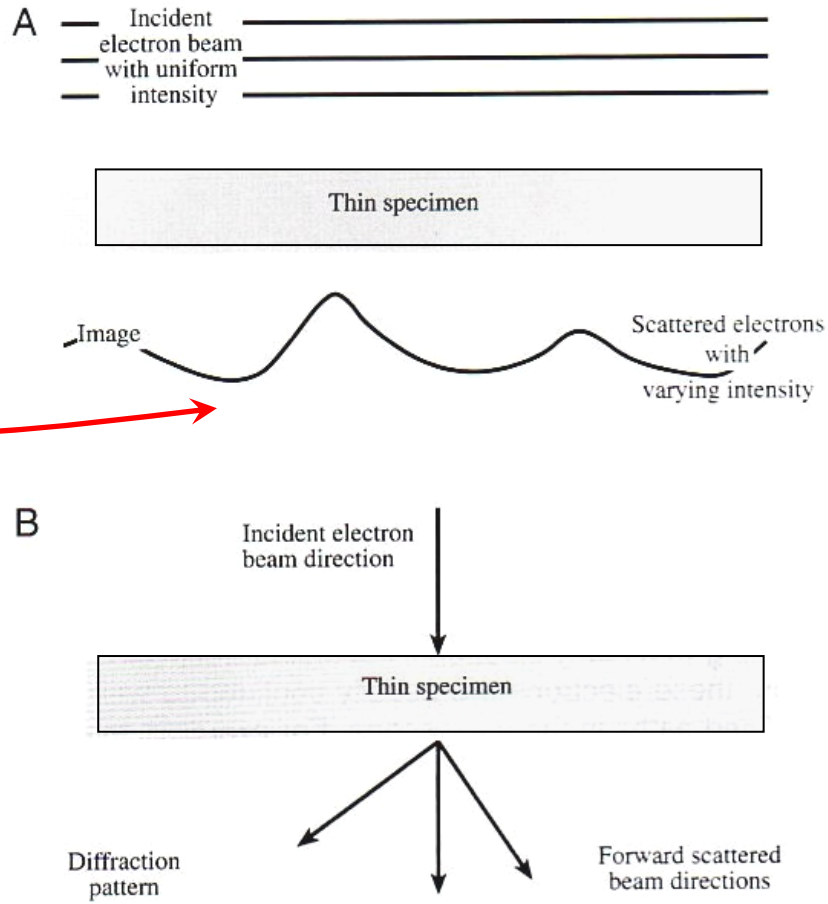

Esta distribución no homogénea de electrones contiene toda la información estructural y química de la muestra

Difracción de electrones

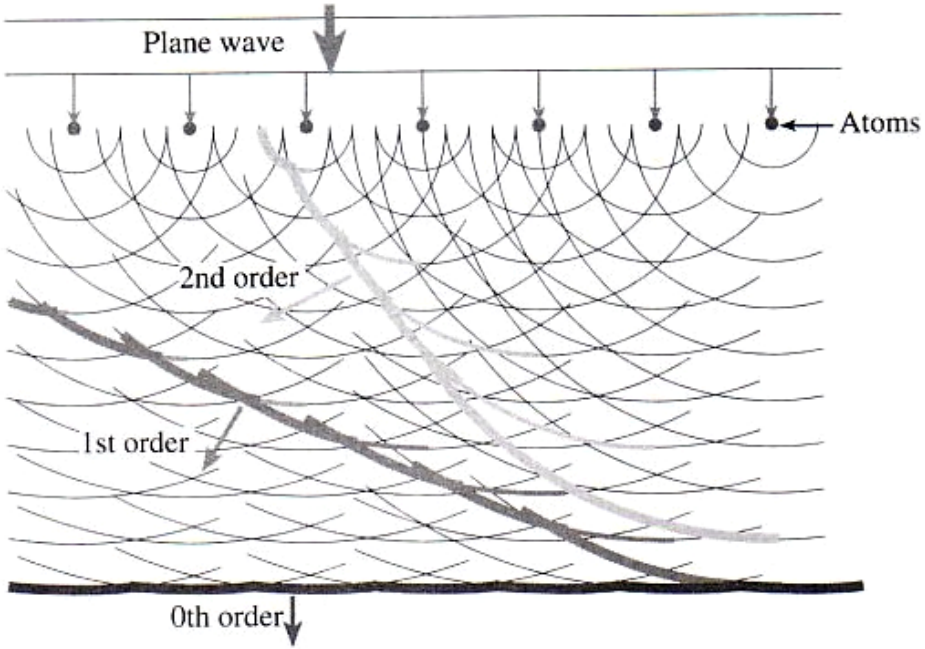

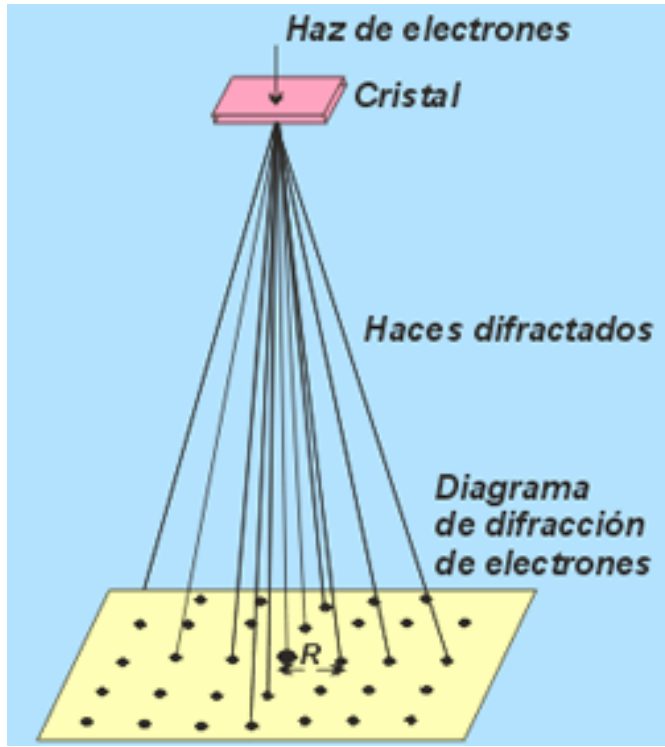

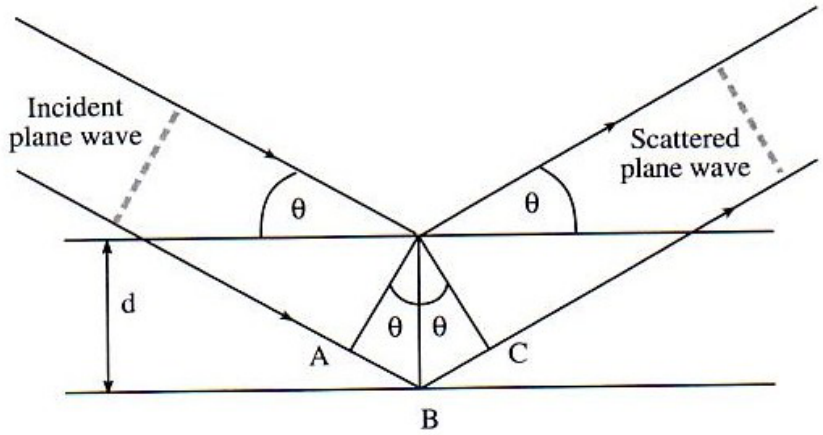

Ley de Bragg $2d \sin\theta_B = n\lambda$

$$\mathbf{K} = \mathbf{k_D} - \mathbf{k_I}$$

$$|\mathbf{k_D}| = |\mathbf{k_I}| = \frac{1}{\lambda} = |\mathbf{k}|$$

$$\sin\theta = \frac{|\mathbf{K}|/2}{|\mathbf{k_I}|}$$

$$|\mathbf{K}| = \frac{2\sin\theta}{\lambda}$$

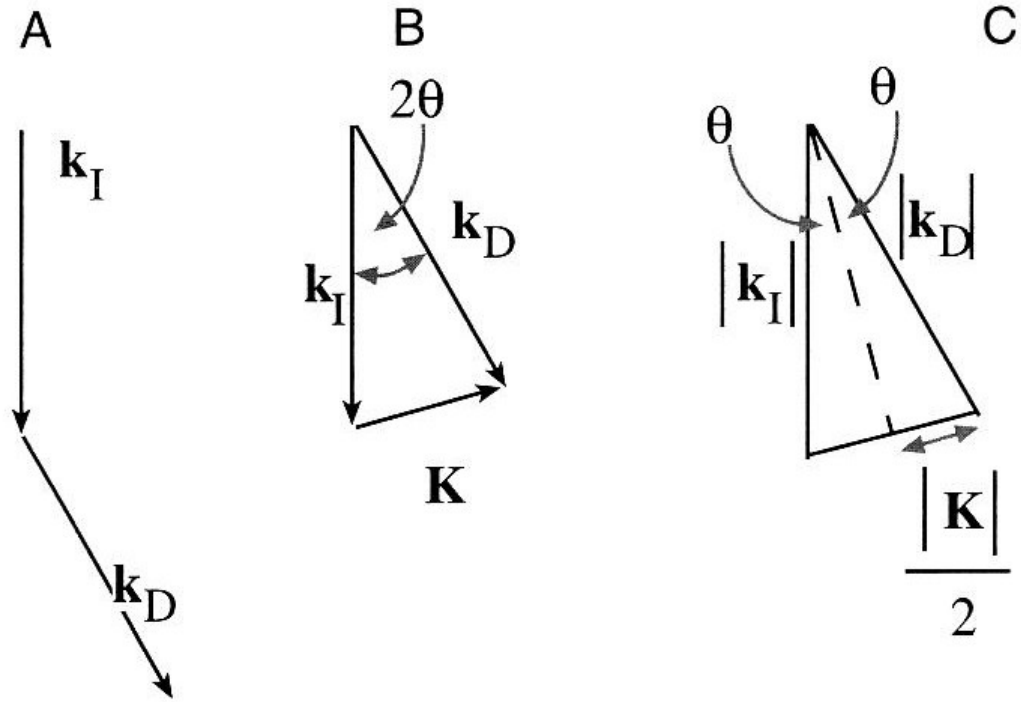

Figure 11.3. Definition of the scattering vectors: (a) the incident wavefront normal is $\mathbf{k}_I$, the diffracted wave normal is $\mathbf{k}_D$; (b) $\mathbf{K}$ is the difference vector ($= \mathbf{k}_D - \mathbf{k}_I$); (c) sin θ is defined as $K/2k_I$.

En el caso de $\theta = \theta_B$:

$$|\mathbf{K}| = \frac{2\sin\theta_B}{\lambda}$$

Ley de Bragg:

$$2\sin\theta_B = \frac{\lambda}{d}$$

$$\Rightarrow \quad |\mathbf{K}_B| = \frac{1}{d}$$

$$\boxed{\mathbf{K}_B = \mathbf{g}}$$

Definición

Espacio recíproco

$$\mathbf{r}_n = n_1\mathbf{a} + n_2\mathbf{b} + n_3\mathbf{c}$$

Vector de red (n_1, n_2 y n_3: enteros)

$$\mathbf{r}^* = m_1\mathbf{a}^* + m_2\mathbf{b}^* + m_3\mathbf{c}^*$$

Vector de red recíproca (m_1, m_2 y m_3: enteros)

$$\mathbf{a}^* \cdot \mathbf{b} = \mathbf{a}^* \cdot \mathbf{c} = \mathbf{b}^* \cdot \mathbf{c} = \mathbf{b}^* \cdot \mathbf{a} = \mathbf{c}^* \cdot \mathbf{a} = \mathbf{c}^* \cdot \mathbf{b} = 0$$

➡ $\mathbf{a}^* \perp \mathbf{b}\ y\ \mathbf{c};\ \mathbf{b}^* \perp \mathbf{a}\ y\ \mathbf{c};\ \mathbf{c}^* \perp \mathbf{a}\ y\ \mathbf{b}$

$$\mathbf{a}^* \cdot \mathbf{a} = \mathbf{b}^* \cdot \mathbf{b} = \mathbf{c}^* \cdot \mathbf{c} = 1$$

➡ Define la magnitud de $\mathbf{a}^*, \mathbf{b}^*, \mathbf{c}^*$

$$\mathbf{a}^* = \frac{\mathbf{b} \times \mathbf{c}}{V_c}$$

Vector **g**

$$\mathbf{K} = \xi \mathbf{a}^* + \eta \mathbf{b}^* + \zeta \mathbf{c}^*$$

$$\mathbf{g}_{hkl} = h\,\mathbf{a}^* + k\,\mathbf{b}^* + l\,\mathbf{c}^*$$

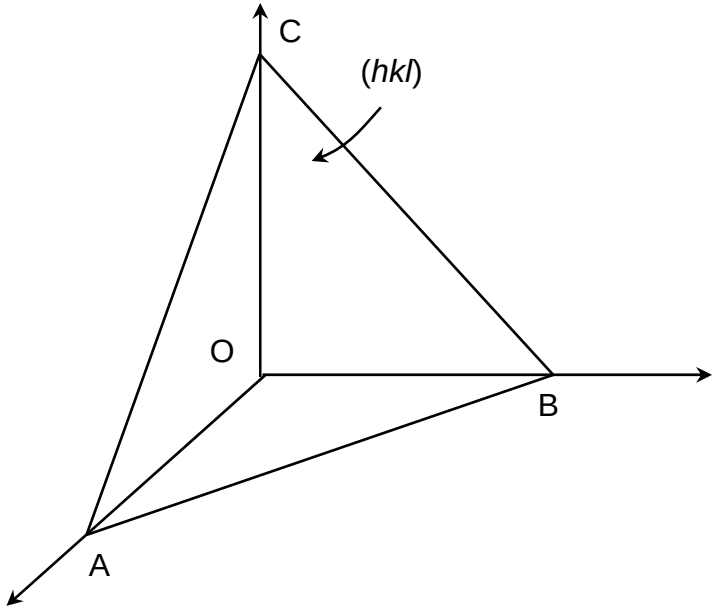

$$\left(\frac{\mathbf{b}}{k} - \frac{\mathbf{a}}{h}\right) \cdot \left(h\,\mathbf{a}^* + k\,\mathbf{b}^* + l\,\mathbf{c}^*\right) = 0 \quad \Rightarrow \quad \mathbf{g}_{hkl} \perp \text{plano}(hkl)$$

$$\mathbf{n} \cdot \frac{\mathbf{a}}{h} = \frac{\mathbf{g}}{|\mathbf{g}|} \cdot \frac{\mathbf{a}}{h} = \frac{\left(h\,\mathbf{a}^* + k\,\mathbf{b}^* + l\,\mathbf{c}^*\right)}{|\mathbf{g}|} \cdot \frac{\mathbf{a}}{h} = \frac{1}{|\mathbf{g}|} \quad \Rightarrow \quad d_{hkl} = \frac{1}{|\mathbf{g}|}$$

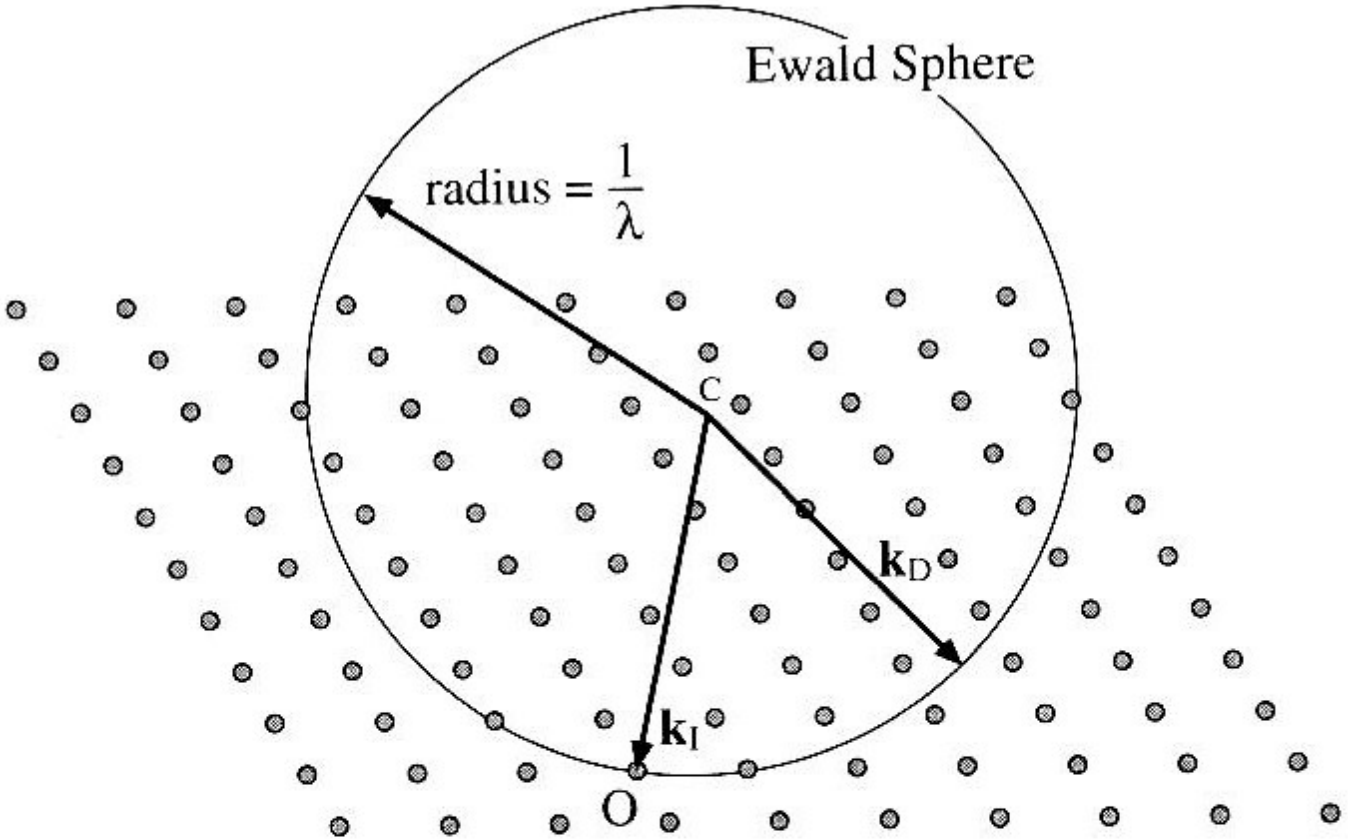

Figure 12.3. The Ewald sphere of reflection is shown intersecting a noncubic array of reciprocal-lattice points. The vector **CO** represents $\mathbf{k}_I$, the wave vector of the incident wave, and O is the origin of the reciprocal lattice. $\mathbf{k}_D$ is any radius vector. When the radius of the sphere is similar to the spacing between the points in the reciprocal lattice, as is the case for X-rays, the sphere can only intersect a few points, as shown. When λ is much smaller, as for 100-keV electrons, the radius is much larger, the sphere is flatter, and it intersects many more points.

Error de excitación

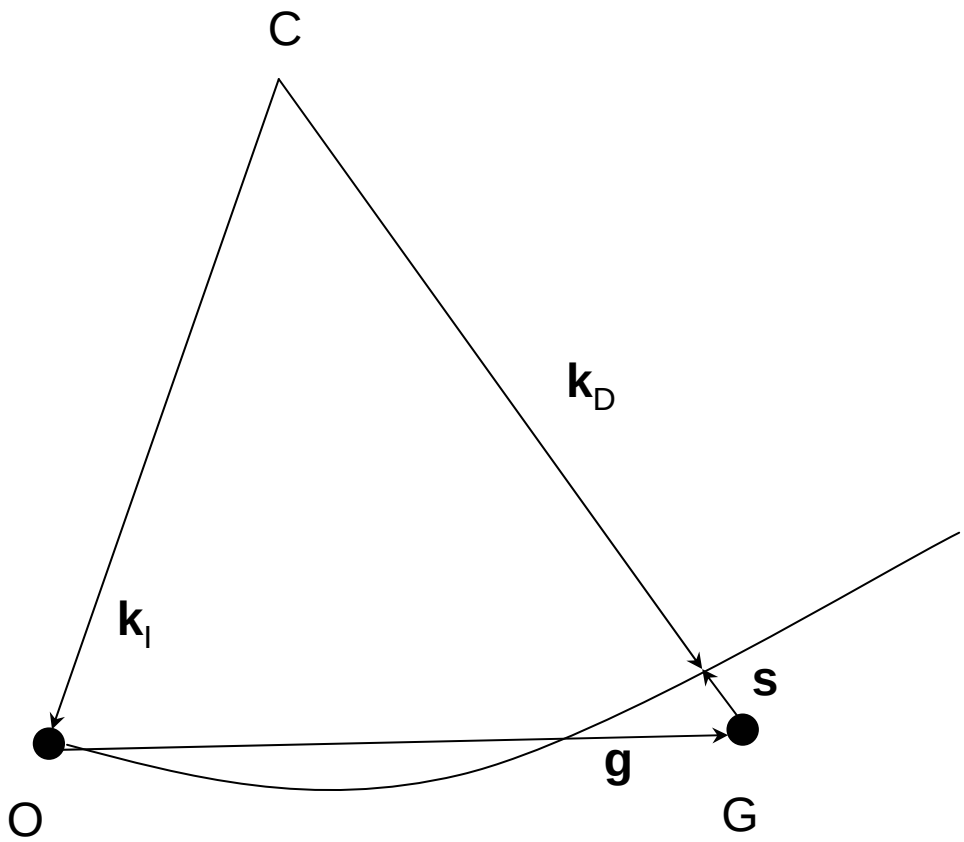

$$\mathbf{K} = \mathbf{g} + \mathbf{s}$$

Difracción de cristales

$$F = \sum_{\mathrm{i}} f_i e^{2\pi i \mathbf{K}\cdot\mathbf{r}_i}$$

Factor de dispersión atómica

$$\mathbf{r}_i = x_i\mathbf{a} + y_i\mathbf{b} + z_i\mathbf{c}$$

Posición atómica

$$\mathbf{K} = h\mathbf{a}^* + k\mathbf{b}^* + l\mathbf{c}^*$$

Vector red recíproca (K=g)

$$F = \sum_{\mathrm{i}} f_i e^{2\pi i\left(hx_i + ky_i + lz_i\right)}$$

Factor de estructura

Difracción de volúmenes finitos

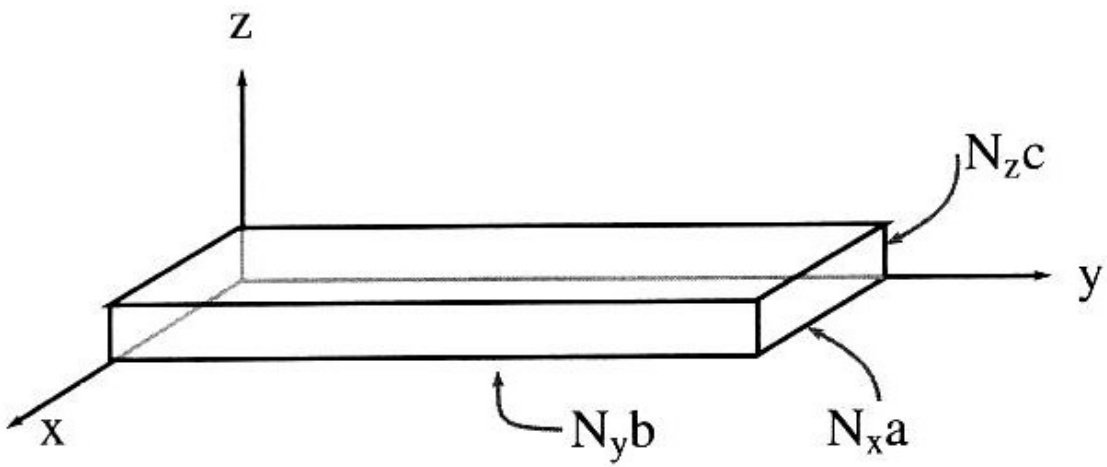

Figure 17.1. An idealized thin-foil specimen modeled as a rectangular slab made up of rectangular unit cells of sides a, b, c. There are N_x cells in the x direction, N_y in the y direction, and N_z in the z direction.

$$A = \sum_{\mathrm{i}} f_i e^{2\pi i \mathbf{K}\cdot\mathbf{r}_i} \sum_{n} e^{2\pi i \mathbf{K}\cdot\mathbf{r}_n}$$

Factor de estructura **Factor de forma**

$$\mathbf{r}_n = n_x\mathbf{a} + n_y\mathbf{b} + n_z\mathbf{c}$$

Posición de cada celda unitaria

$$A = F\sum_{n_x} e^{2\pi i n_x \mathbf{K}\cdot\mathbf{a}} \sum_{n_y} e^{2\pi i n_y \mathbf{K}\cdot\mathbf{b}} \sum_{n_z} e^{2\pi i n_z \mathbf{K}\cdot\mathbf{c}}$$

$$\sum_{n_x=0}^{n_x=N-1} e^{2\pi i n_x K\cdot a} = \frac{1-e^{2\pi i n_x K\cdot a}}{1-e^{2\pi i K\cdot a}}$$

$$I = |A|^2 = |F|^2 \left(\frac{\sin(\pi N_x K\cdot \mathbf{a})}{\sin^2(\pi K\cdot \mathbf{a})}\right)\left(\frac{\sin(\pi N_y K\cdot \mathbf{b})}{\sin^2(\pi K\cdot \mathbf{b})}\right)\left(\frac{\sin(\pi N_z K\cdot \mathbf{c})}{\sin^2(\pi K\cdot \mathbf{c})}\right)$$

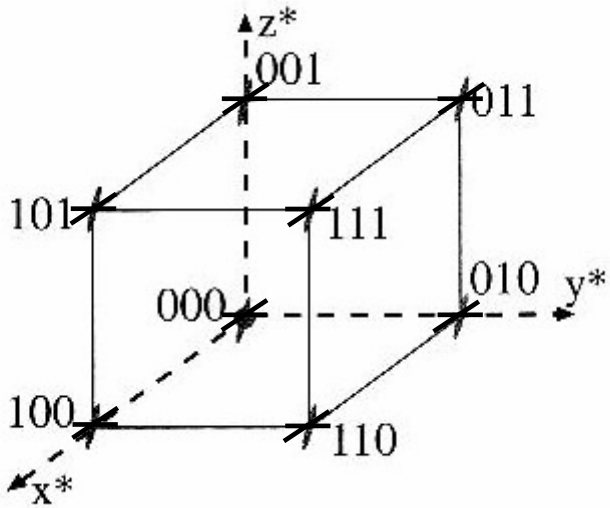

Relrods

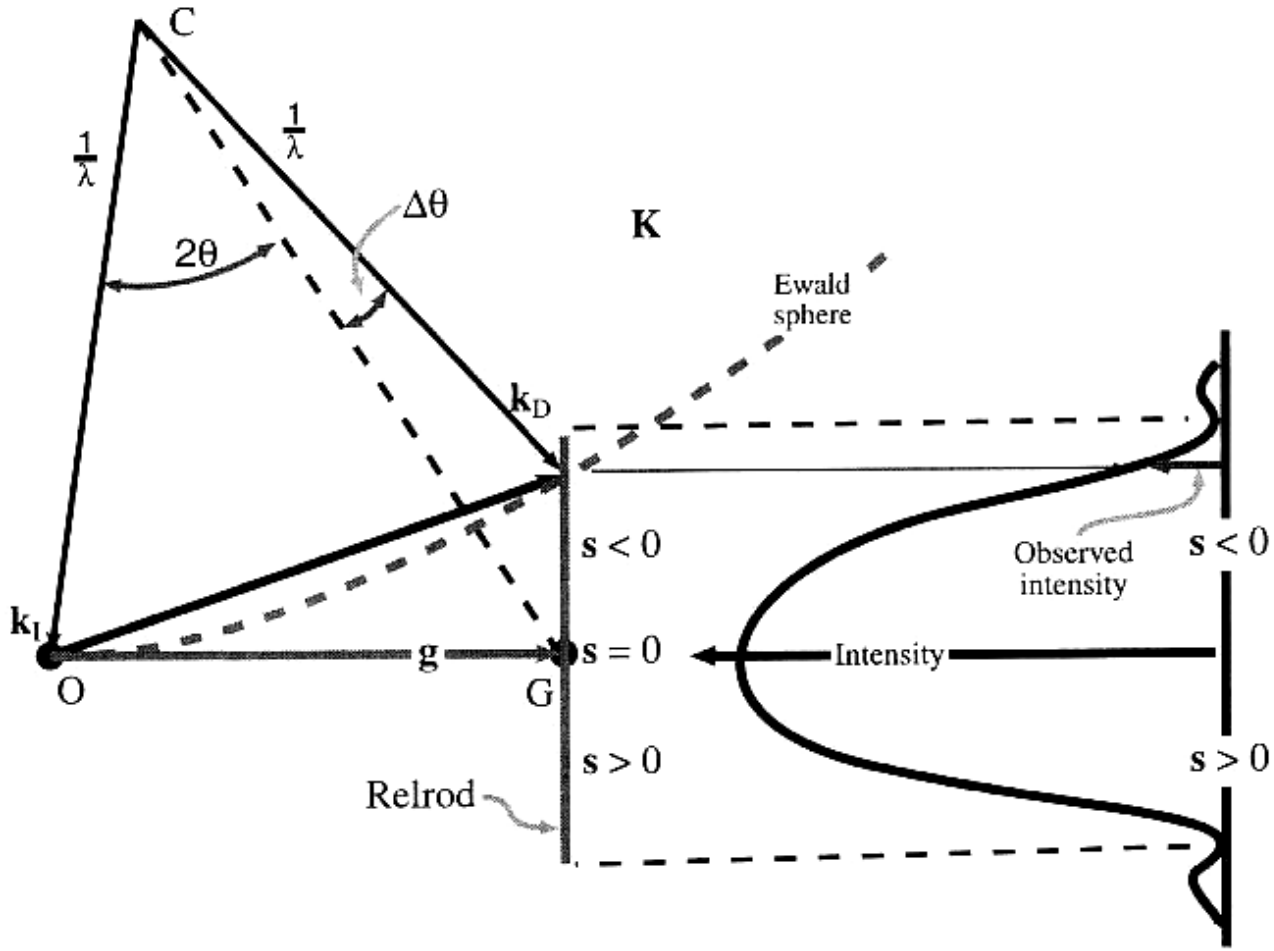

Figure 17.2. The relrod at $\mathbf{g}_{hk\ell}$ when the beam is $\Delta\theta$ away from the exact Bragg condition. The Ewald sphere intercepts the relrod at a negative value of **s** which defines the vector $\mathbf{K} = \mathbf{g} + \mathbf{s}$. The intensity of the diffracted beam as a function of where the Ewald sphere cuts the relrod is shown on the right of the diagram. In this case the intensity has fallen almost to zero.

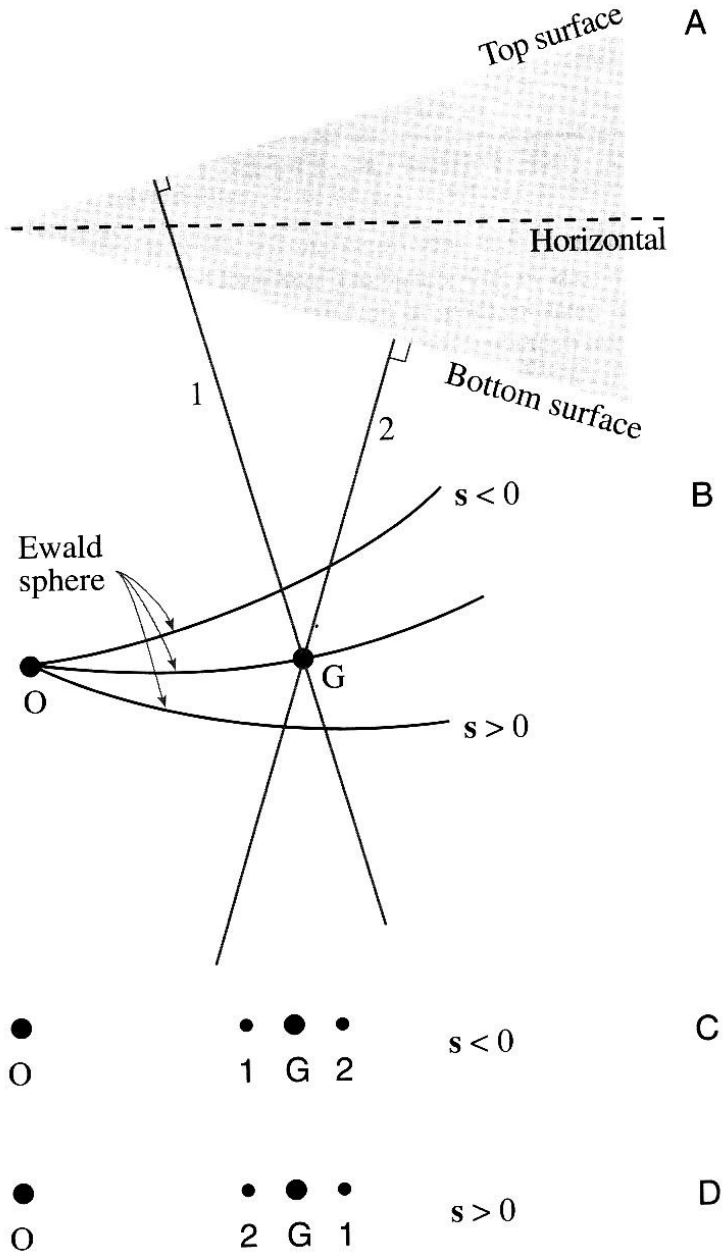

Figure 17.4. (A) Diffraction from a wedged crystal. (B) Notice that when $s < 0$, relrod 1 is on the left of relrod 2 but the order reverses when s becomes >0. The effect of this pair of relrods is to create a doublet shown in (C) and (D). The middle spot is the matrix relrod.

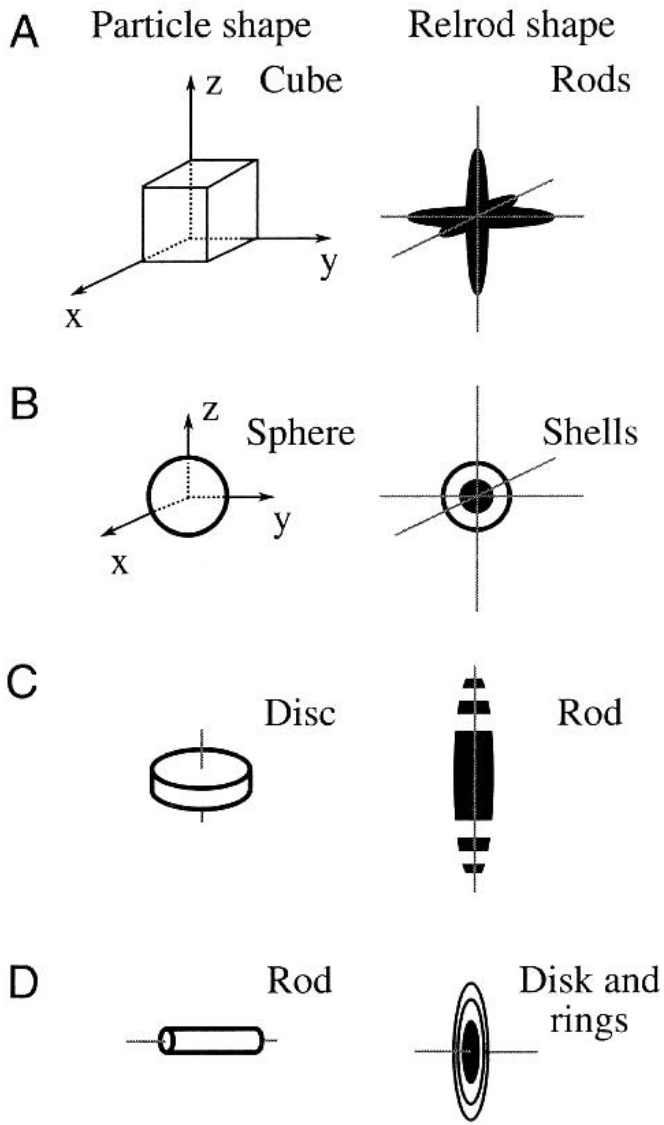

Figure 17.9. Examples of how spots in reciprocal space have different shapes, depending on the shape of the particles which are diffracting.

Haces Difractados

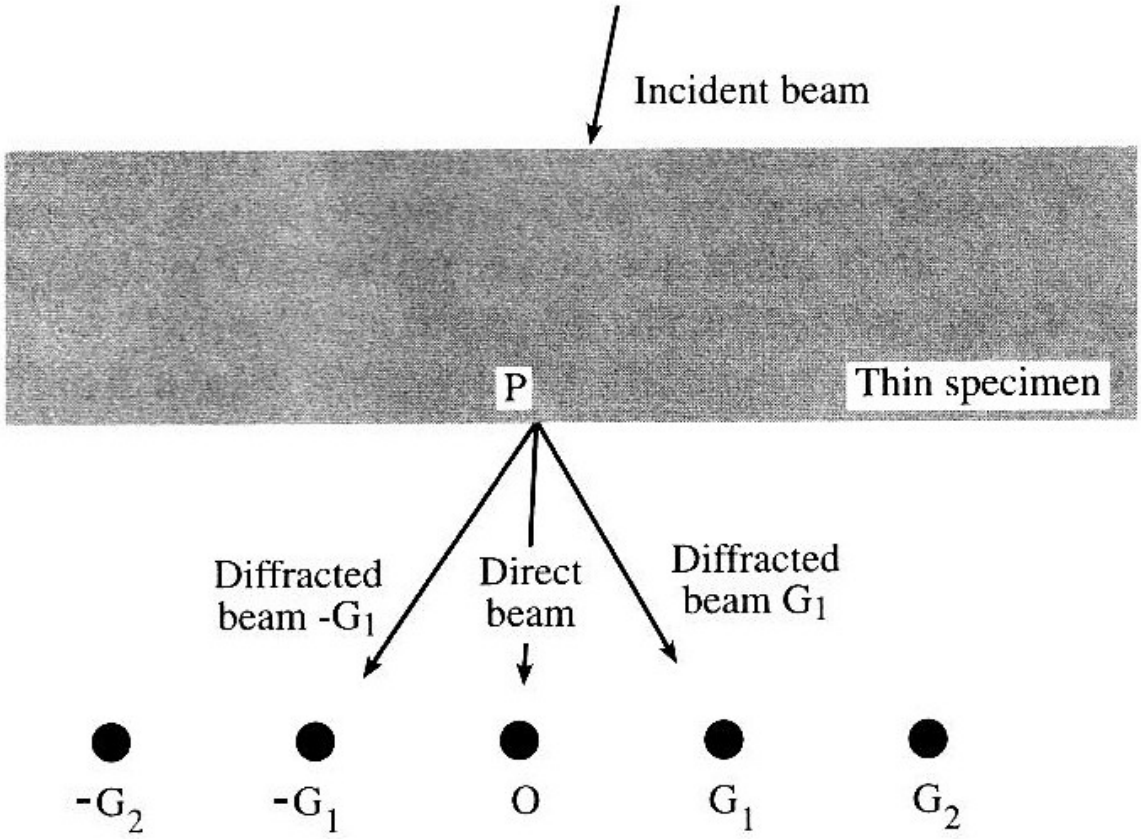

Figure 13.1. Defining the point P. The incident beam is scattered inside the thin specimen. We want to know the intensities of the direct beam (O) and the diffracted (G_i) beams for each point P at the bottom surface of the specimen (the exit surface).

Representación de la onda de electrones

$$\psi^{T} = \phi_0 e^{2\pi i \chi_0 \cdot \mathbf{r}} + \phi_{\mathbf{g_1}} e^{2\pi i \chi_{\mathbf{g1}} \cdot \mathbf{r}} + \phi_{\mathbf{g_2}} e^{2\pi i \chi_{\mathbf{g2}} \cdot \mathbf{r}} + \cdots$$

χ Vector de onda en el vacío

$\mathbf{k}$ Vector de onda en la muestra

Necesitamos conocer la amplitud de los haces difractados

Ecuaciones de Howie-Whelan

$$\frac{d\phi_{\mathbf{g}}}{dz} = \frac{\pi i}{\xi_{\mathbf{g}}}\phi_{\mathbf{0}} e^{-2\pi isz} + \frac{\pi i}{\xi_{\mathbf{0}}}\phi_{\mathbf{g}}$$

$$\frac{d\phi_{\mathbf{0}}}{dz} = \frac{\pi i}{\xi_{\mathbf{0}}}\phi_{\mathbf{0}} + \frac{\pi i}{\xi_{\mathbf{g}}}\phi_{\mathbf{g}} e^{-2\pi isz}$$

Difracción dinámica en condición de dos haces

$$\left|\phi_{\mathbf{g}}\right|^2 = \left(\frac{\pi t}{\xi_{\mathbf{g}}}\right)^2 \frac{\sin^2\left(\pi t s_{eff}\right)}{\left(\pi t s_{eff}\right)^2}$$

Intensidad del haz difractado

$$s_{eff} = \sqrt{s^2 + \frac{1}{\xi_{\mathbf{g}}^2}}$$

Error de excitación efectivo

Analogía con un oscilador armónico

Cuando s=0, la intensidad del haz difractado y directo corresponde a:

$$\left|\phi_{\mathbf{g}}\right|^2 = \sin^2\left(\frac{\pi t}{\xi_{\mathbf{g}}}\right)$$

$$\left|\phi_{\mathbf{0}}\right|^2 = 1 - \sin^2\left(\frac{\pi t}{\xi_{\mathbf{g}}}\right)$$

Notamos que I_g es cero en t=0 y nuevamente en $t=\xi_g$.

Por esta razón ξ_g se denomia **distancia de extinción**: es la distancia a la cual la intensidad del haz difractado se hace nula

La intensidad es continuamente transferida desde I_0 a I_g y viceversa a medida que cambia el espesor.

Ecuación de Schrödinger

$$\nabla^2\Psi(\mathbf{r}) + \frac{8\pi^2 me}{h^2}\left[E + V(\mathbf{r})\right]\Psi(\mathbf{r}) = 0$$

$$V(\mathbf{r}) = V(\mathbf{r}+\mathbf{R})$$

$$V(\mathbf{r}) = \sum_{\mathbf{g}} V_{\mathbf{g}} e^{2\pi i \mathbf{g}\cdot\mathbf{r}}$$

$$V_{\mathbf{g}} = \frac{h^2}{2me} U_{\mathbf{g}}$$

$$V(\mathbf{r}) = \frac{h^2}{2me} \sum_{\mathbf{g}} U_{\mathbf{g}} e^{2\pi i \mathbf{g}\cdot\mathbf{r}}$$

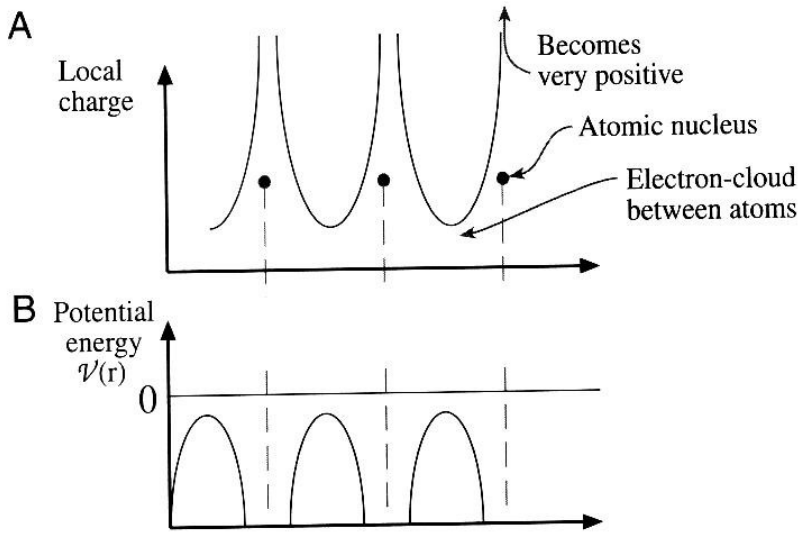

Figure 14.1. (A) The local charge sensed by the beam electron as it passes through a metal, represented as a row of "ion" cores (black circles) in a sea of electrons. The local charge is very large and positive in the vicinity of the ion and becomes small, but not zero, between the ions. The difference between the minimum charge and zero corresponds to the mean inner potential of the crystal, which is a few eV (positive). So the beam electron experiences a small positive attraction as it enters the crystal, hence its kinetic energy (velocity) increases. (B) $V(\mathbf{r})$ is the potential of the electrons, so their potential *energy* is negative and becomes more so, the closer they pass by the ions.

Ondas de Bloch

$$\Psi^{(j)}(\mathbf{r}) = \sum_{\mathbf{g}} C_{\mathbf{g}}^{(j)} e^{2\pi i(\mathbf{k}^{(j)}+\mathbf{g})\cdot\mathbf{r}}$$

Poseen la simetría del cristal

$$\Psi_{total} = \sum_{j=1}^{n} A^{(j)}\Psi^{(j)}(\mathbf{r})$$

Representación en función de ondas de Bloch

$$\Psi_{total} = \sum_{j=1}^{n} \phi_j e^{2\pi i\mathbf{k}\cdot\mathbf{r}}$$

Representación en función de haces difractados

➡

ϕ_0 está compuesta de $\Psi^{(1)}$ y $\Psi^{(2)}$

$\phi_{\mathbf{g}}$ está compuesta de $\Psi^{(1)}$ y $\Psi^{(2)}$

Condición de dos haces

$$\phi_{\mathbf{g}} = \sin\frac{\beta}{2}\cos\frac{\beta}{2}\left\{\underbrace{e^{2\pi i\left(\mathbf{k}^{(2)}-\mathbf{K}\right)\cdot\mathbf{r}}}_{\Psi^{(2)}} - \underbrace{e^{2\pi i\left(\mathbf{k}^{(1)}-\mathbf{K}\right)\cdot\mathbf{r}}}_{\Psi^{(1)}}\right\}$$

Usando las ondas de Bloch se define la distancia de extinción como:

$$\xi_{\mathbf{g}} = \frac{2\kappa\cos\theta_B}{U_g} = \frac{1}{\left|\mathbf{k}^{(2)}-\mathbf{k}^{(1)}\right|}$$

$$\kappa^2 = \frac{2meE}{h^2} + U_0$$

Vector de onda dentro del cristal

Distancia de extinción

Distancia a la cual la intensidad del haz incidente se transfiere completamente al haz difractado

$$\left|\phi_{\mathbf{g}}\right|^2 = \sin^2\left(\frac{\pi t}{\xi_{\mathbf{g}}}\right)$$

Es el “latido” de las ondas de Bloch

$$\left|\phi_{\mathbf{0}}\right|^2 = 1-\sin^2\left(\frac{\pi t}{\xi_{\mathbf{g}}}\right)$$

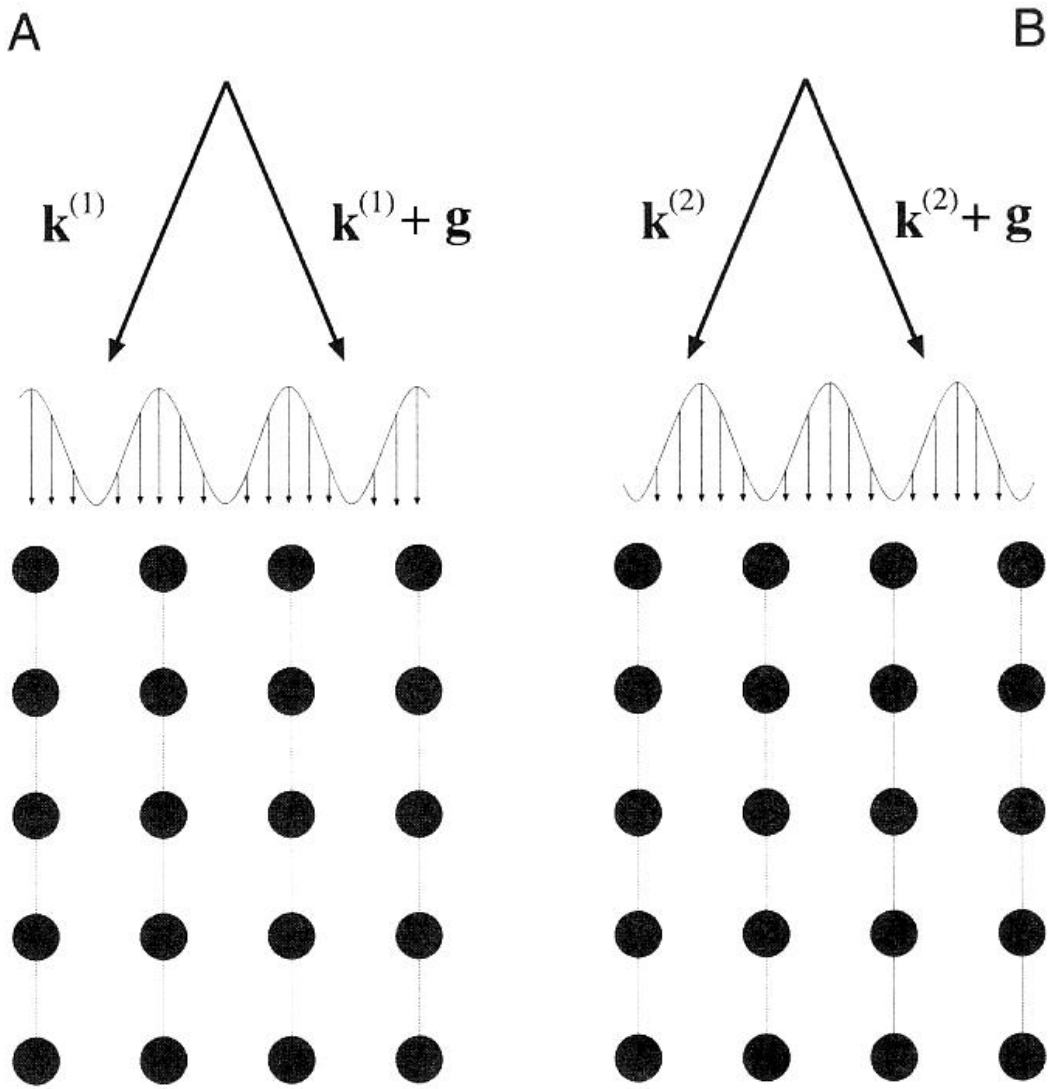

Figure 14.2. The two types of Bloch wave in the crystal aligned at the Bragg condition: (A) the maximum lies along the ion cores and Bloch wave 1 interacts strongly; (B) the maximum lies between the ions so that the interactions are weaker.

Patrones de Difracción

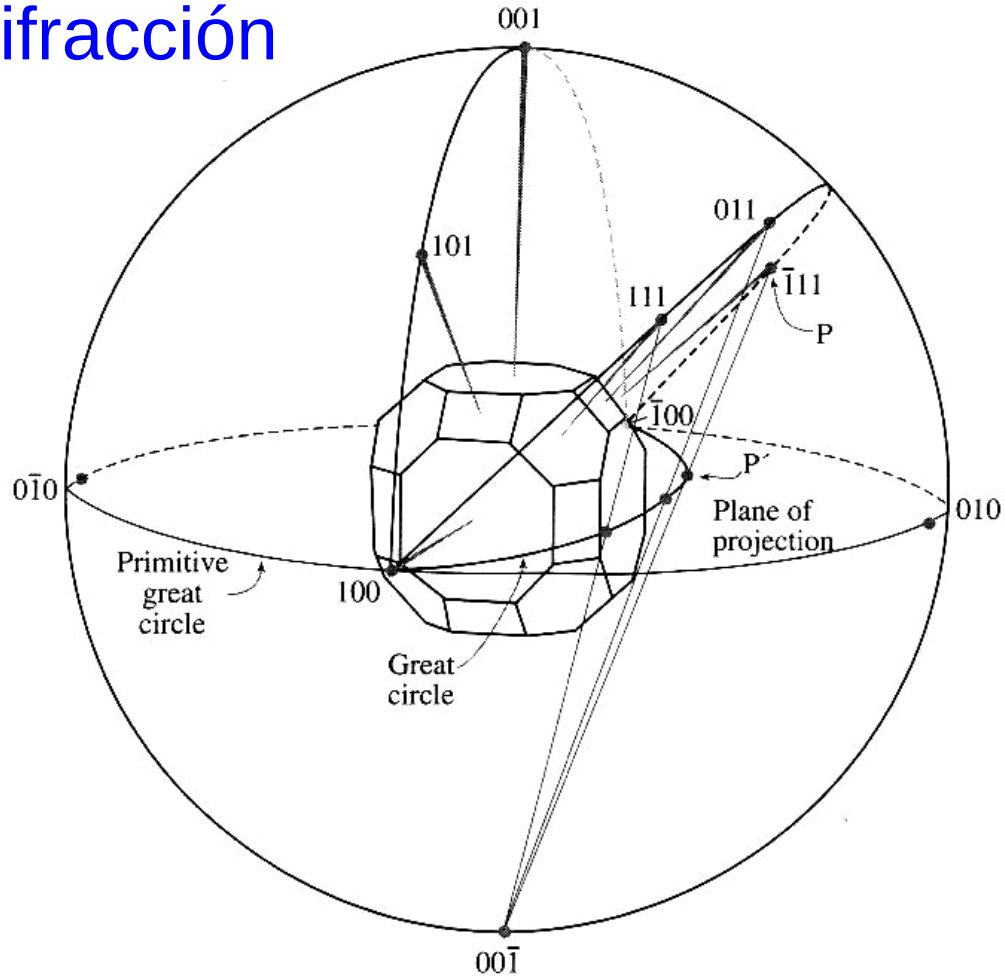

Figure 18.2. The stereographic projection. The crystal is at the center of the sphere. Normals to the crystal planes are projected until they intercept the sphere at P, then projected back to the south pole $(00\bar{1})$ of the sphere. Where this projected line crosses the equatorial plane at P' is the point that uniquely represents the original plane on the crystal. Note that planes in the same zone on the crystal project as a line of longitude on the sphere, called a great circle, and project as the arc of a circle on the equatorial plane, whose circumference is called the primitive great circle.

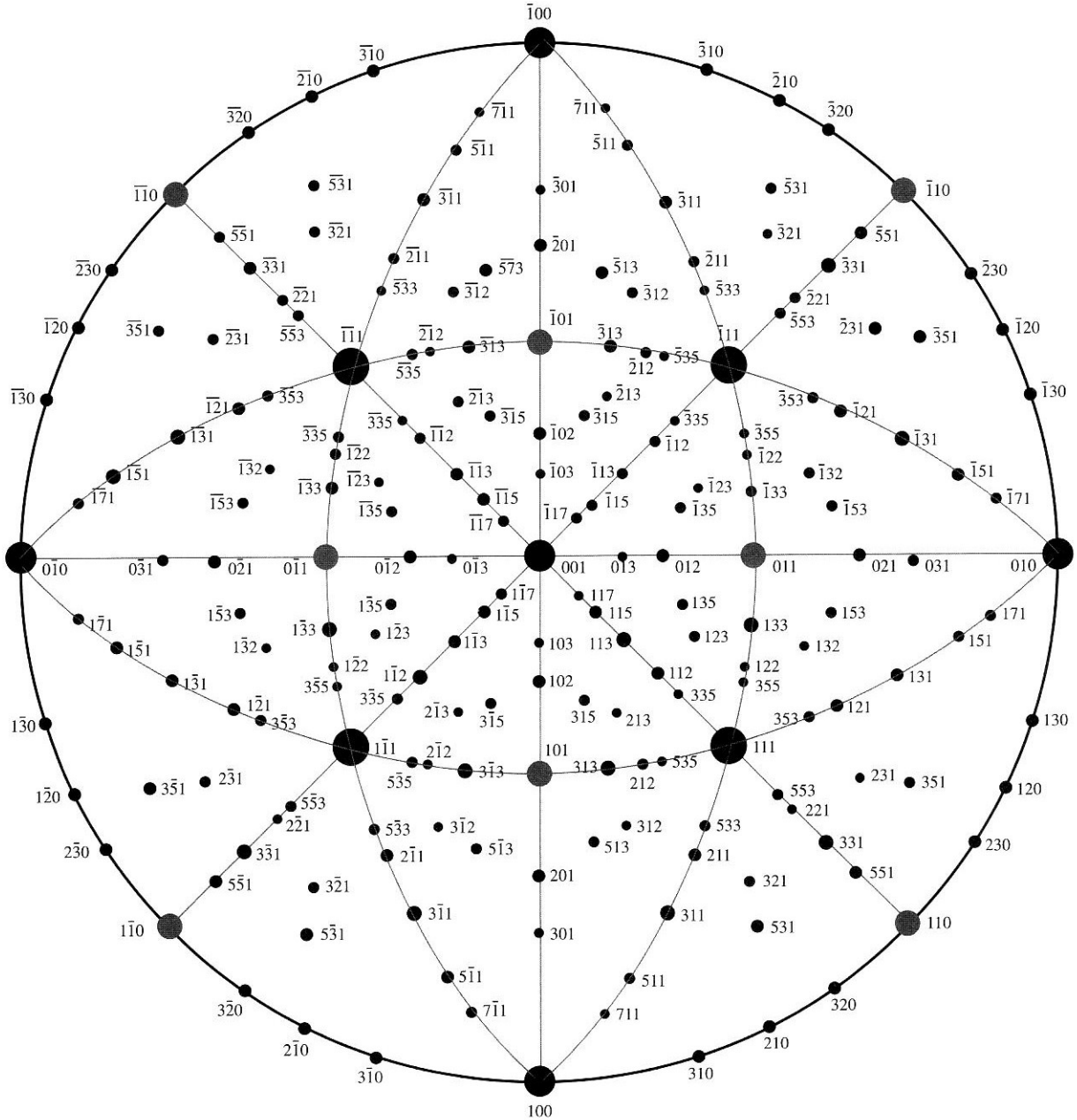

Figure 18.5. The stereographic projection for a cubic foil with a [001] normal, assuming the beam is down [001] also. If you want to form an image with the $0\bar{2}2$ reflection, you need to tilt the specimen so the $0\bar{1}1$ pole rotates until it is on the primitive, i.e., it is 90° from the beam direction. To do this you need to tilt about an axis that is 90° from the $0\bar{2}2$ reflection, such as the [100], [111], [311], zone axes.

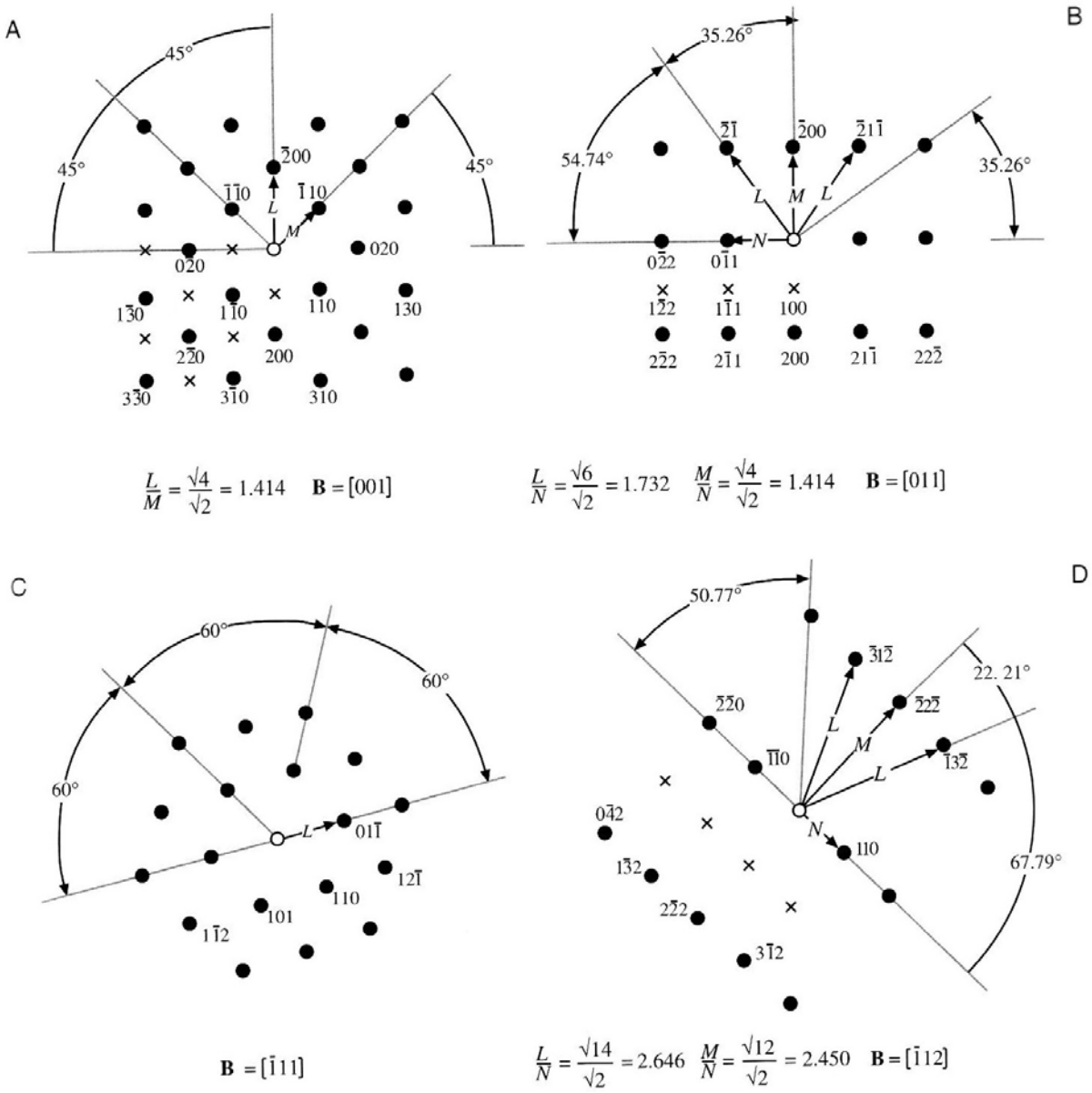

Figure 18.17. Four standard indexed diffraction patterns for bcc crystals in the [001], [011], $[\bar{1}11]$, and $[\bar{1}12]$ beam directions. Ratios of the principal spot spacings are shown as well as the angles between the principal plane normals. Forbidden reflections are indicated by x.

$$Rd = \lambda L$$

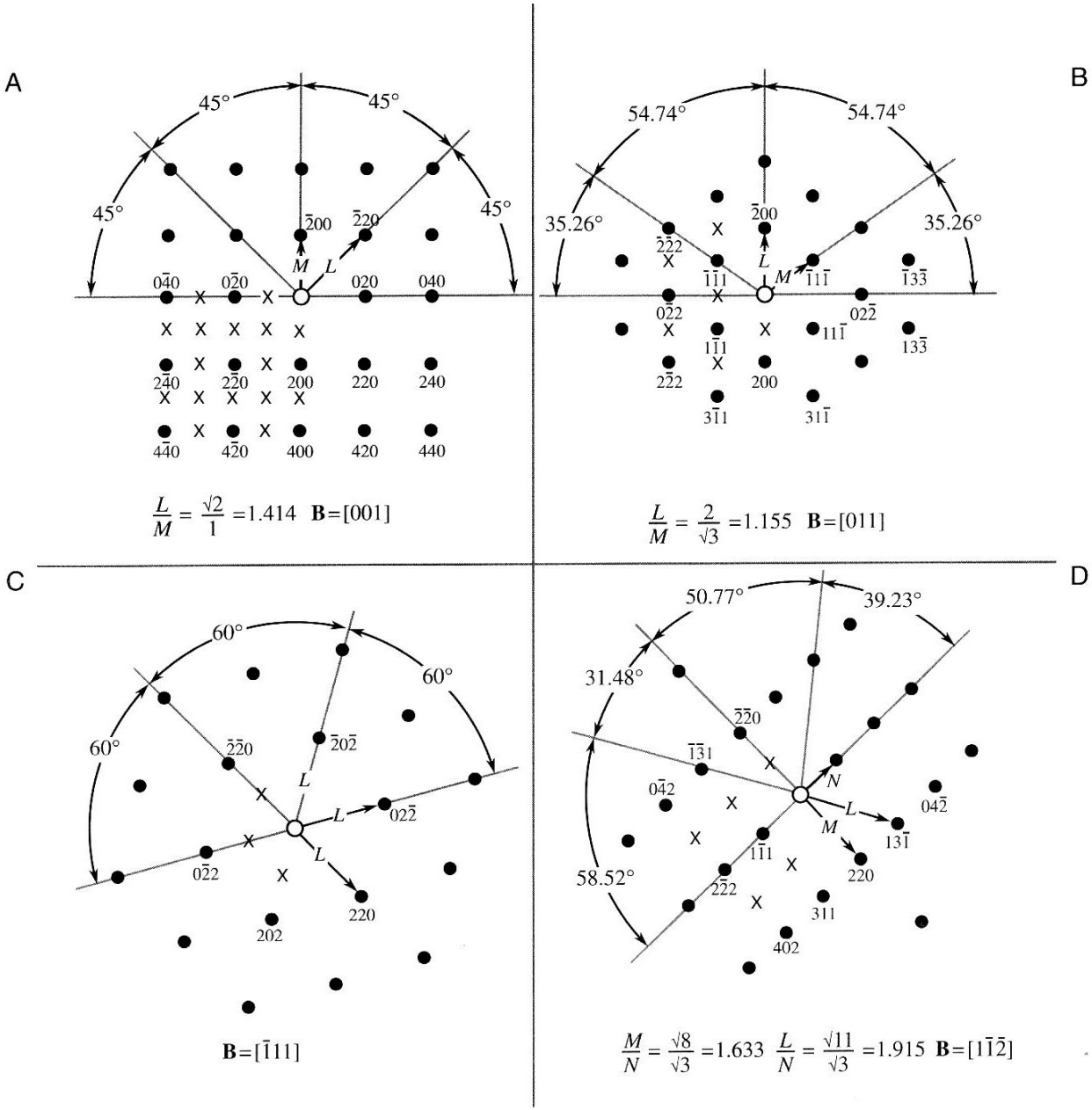

Figure 18.18. Four standard indexed diffraction patterns for fcc crystals in the [001], [011], [$\bar{1}$11], and [$\bar{1}$12] beam directions. Ratios of the principal spot spacings are shown as well as the angles between the principal plane normals. Forbidden reflections are indicated by x.

Ejemplos

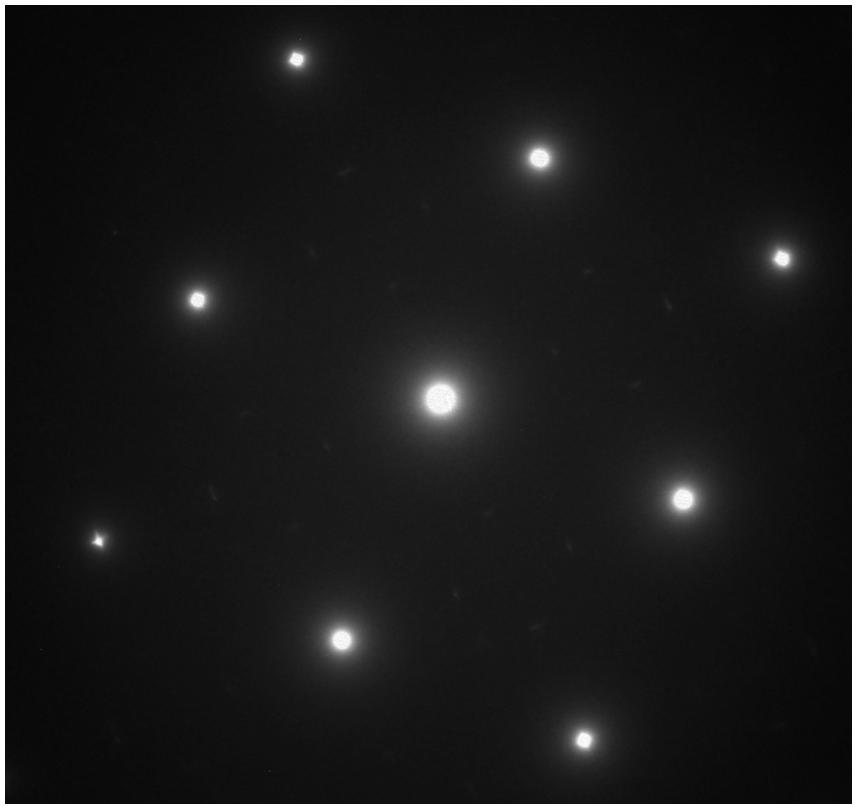

Al

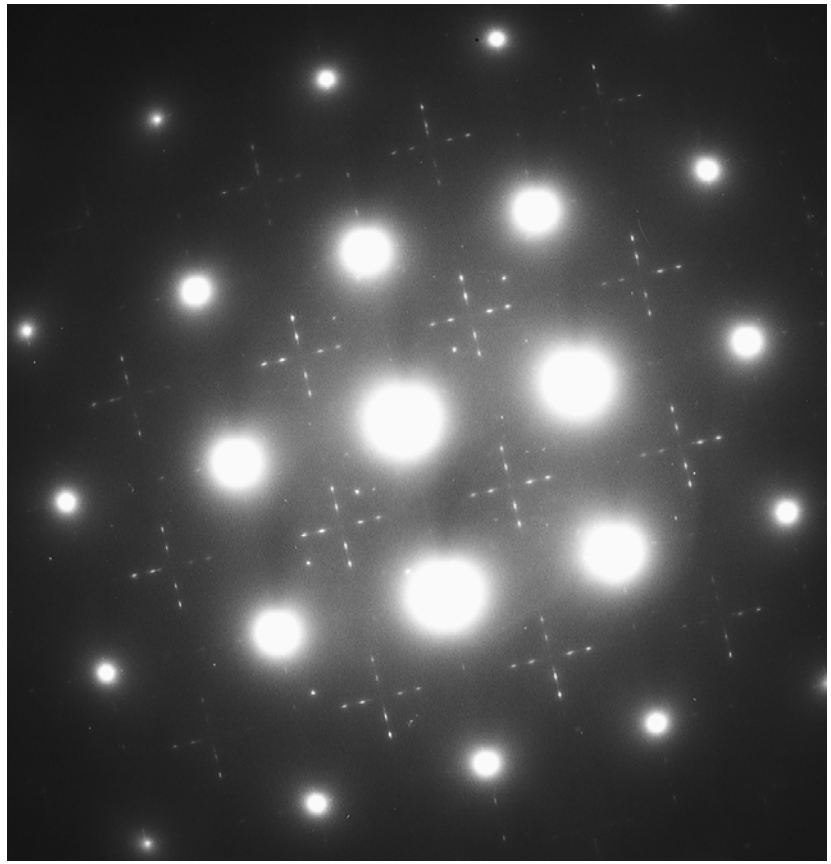

Al-Cu-Mg

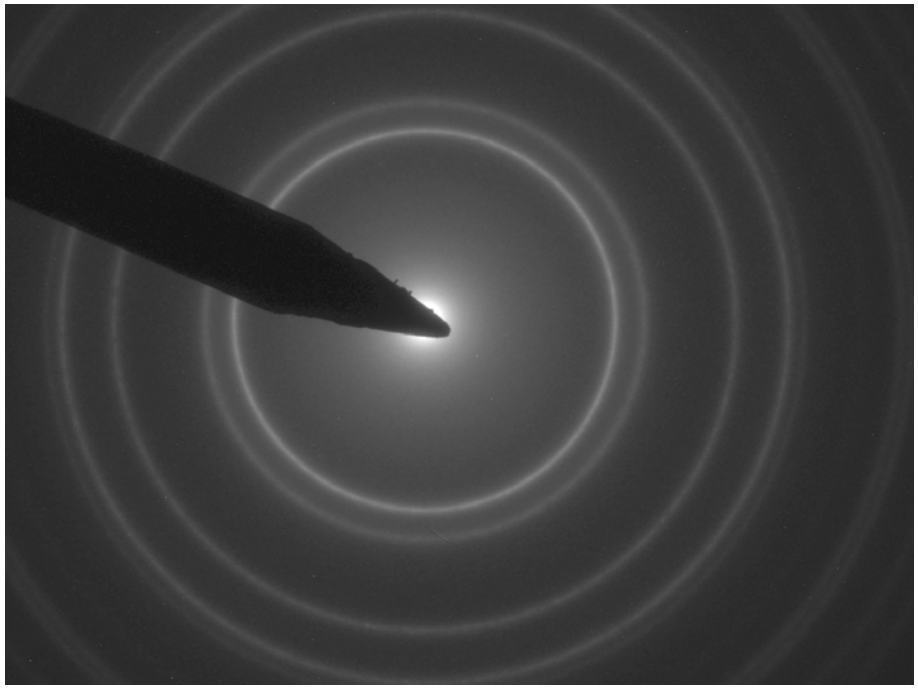

Nanopartículas de Oro

2-3 nm

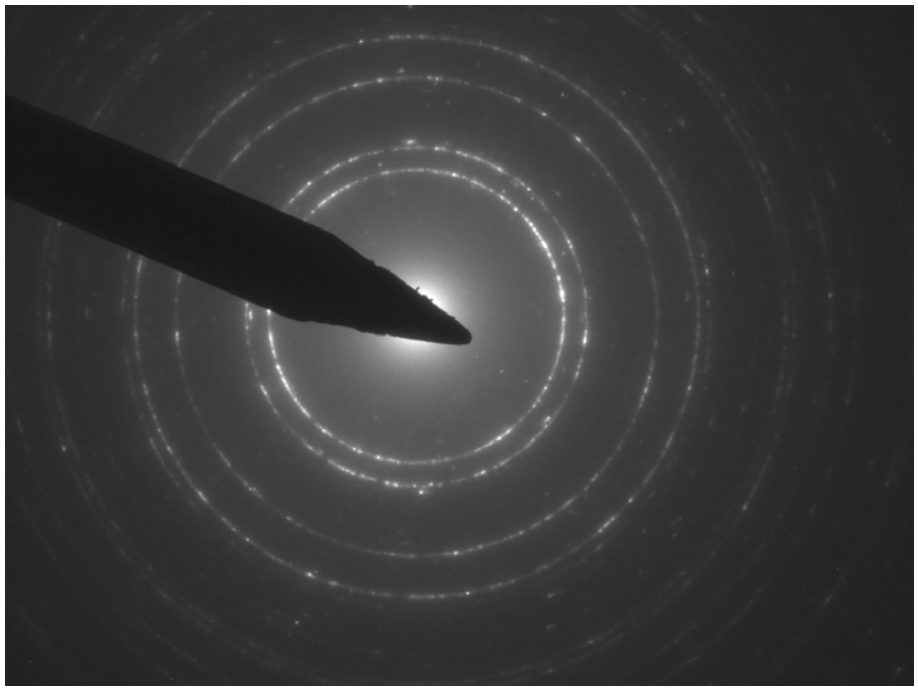

Aluminio nanocrisrtalino

30-50 nm

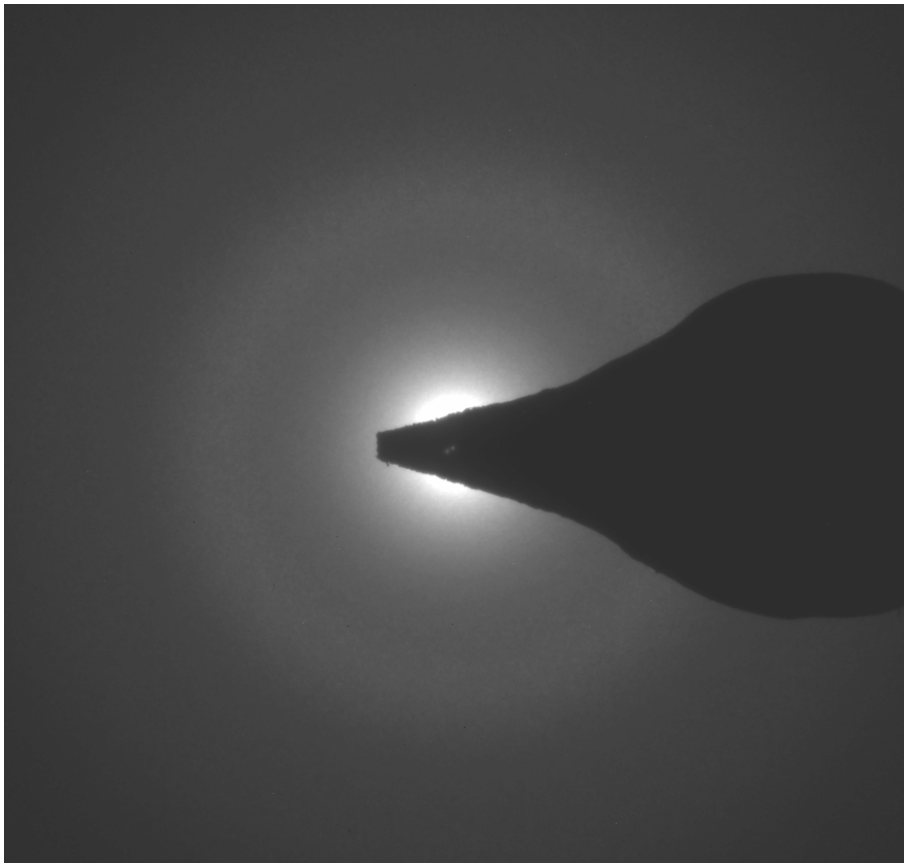

SiC amorfo

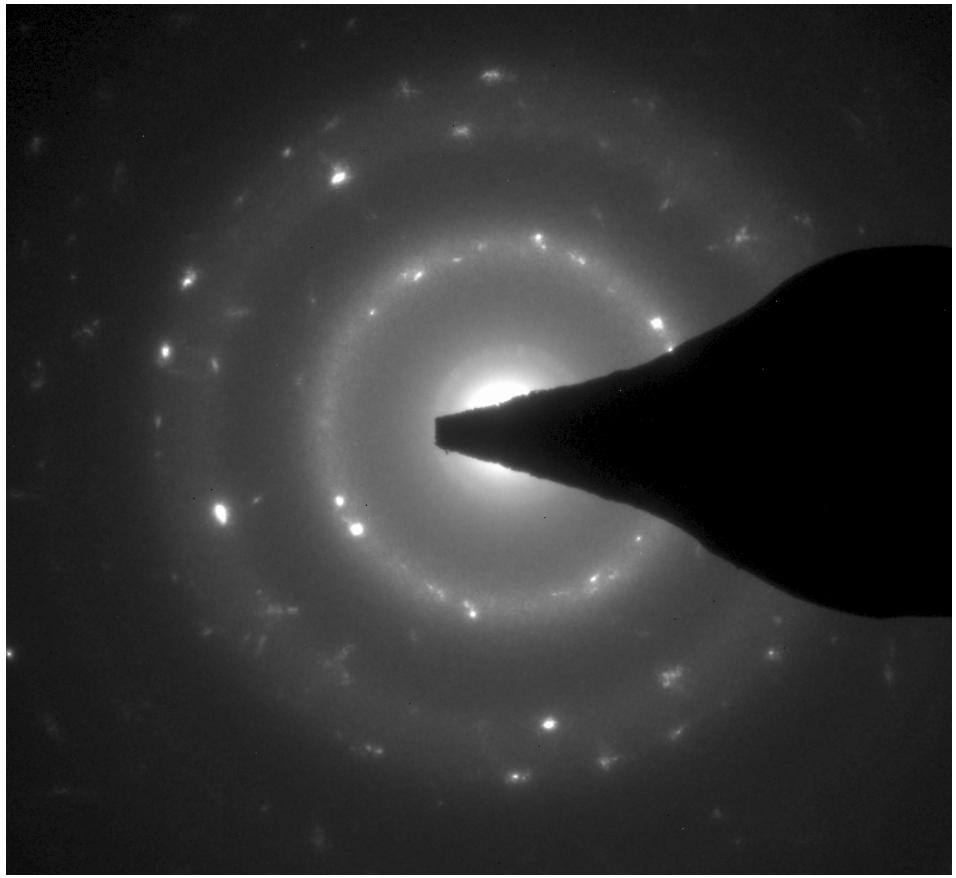

SiC parcialmente cristalizado

Convergent-Beam Electron Diffraction CBED

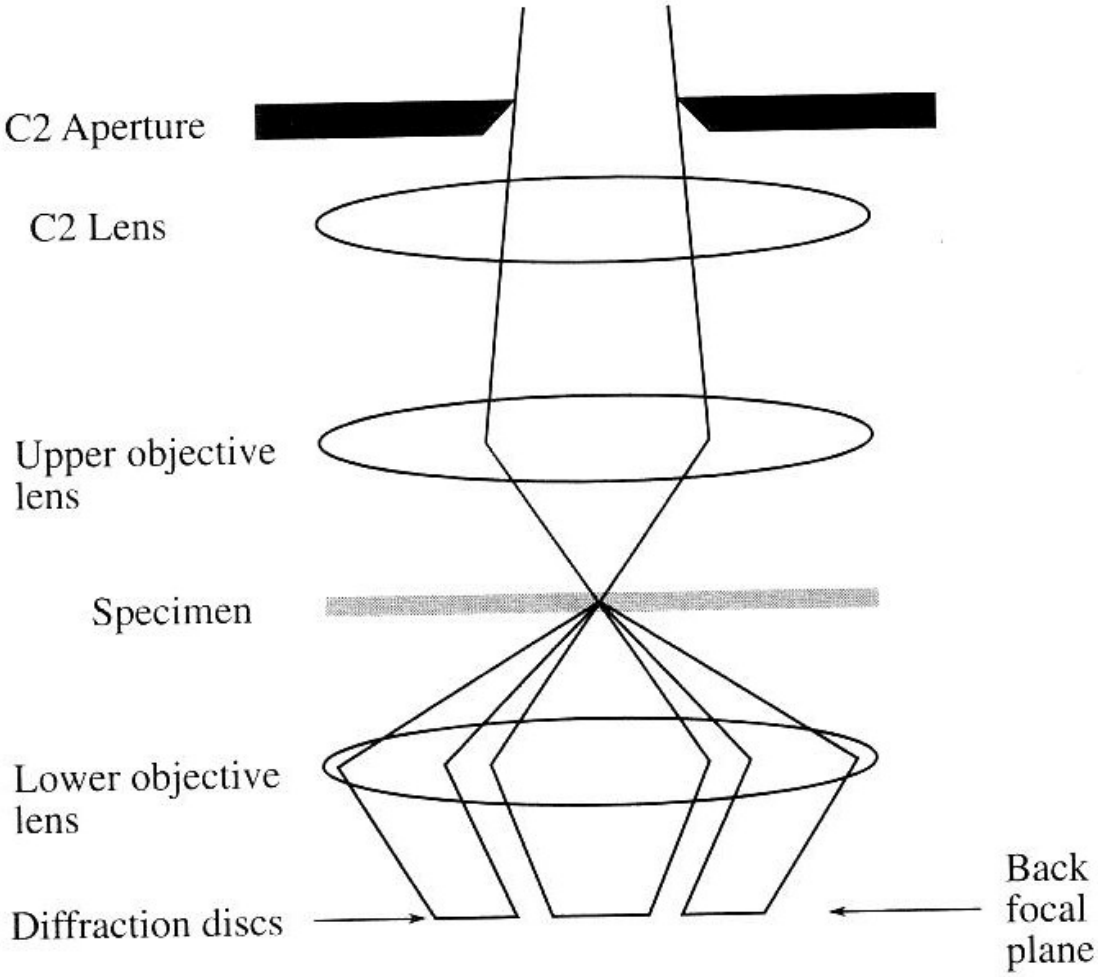

Figure 20.1. Ray diagram showing CBED pattern formation. A convergent beam at the specimen results in the formation of disks in the BFP of the objective lens.

Convergent-Beam Electron Diffraction CBED

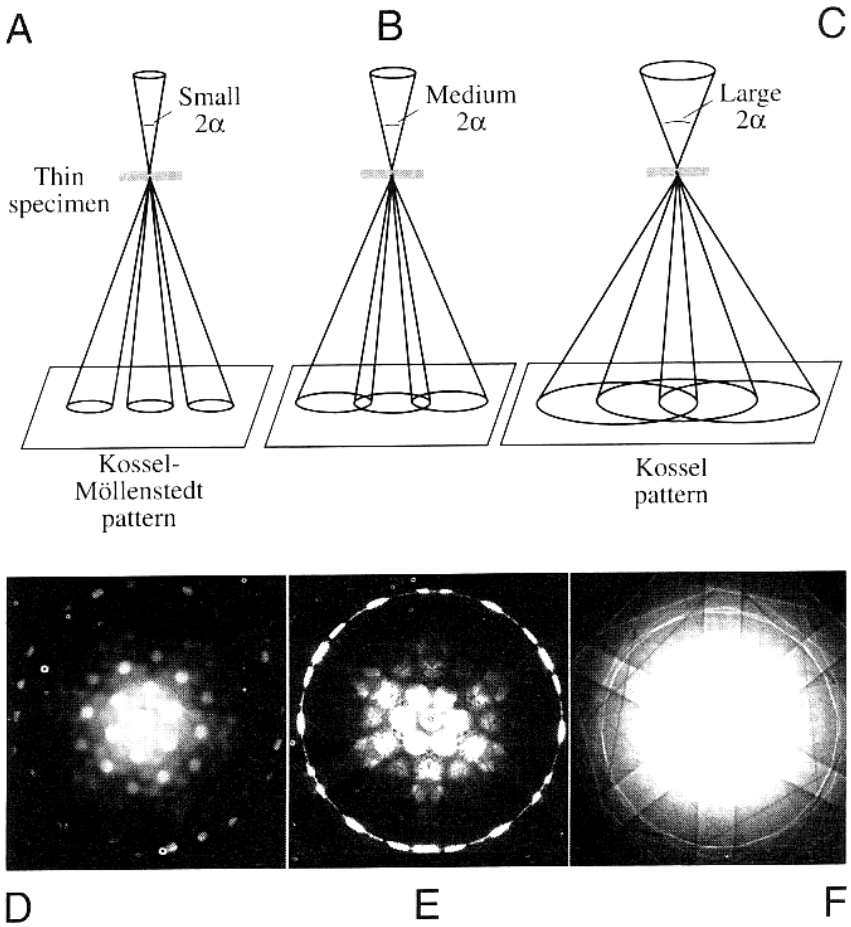

Figure 20.3. (A)–(C) Ray diagrams showing how increasing the C2 aperture size causes the CBED pattern to change from one in which individual disks are resolved to one in which all the disks overlap. In (D)–(F) you can see what happens to experimental patterns on the TEM screen as you select larger C2 apertures.

Con iluminación paralela podemos analizar regiones de la muestra de ~500 nm

Con CBED podemos obtener información cristalográfica de regiones mucho más pequeñas (1 a 10 nm)

Además tenemos acceso a información que no está disponible en experimentos convencionales de difracción:

- Espesor de la muestra
- Celda unitaria y determinación precisas de parámetros de red
- Sistema cristalino y simetría tridimensional real

Las desventajas de esta técnica son:

- Contaminación localizada
- Calentamiento o daño de la zona analizada

Comparación entre SAD y CBED

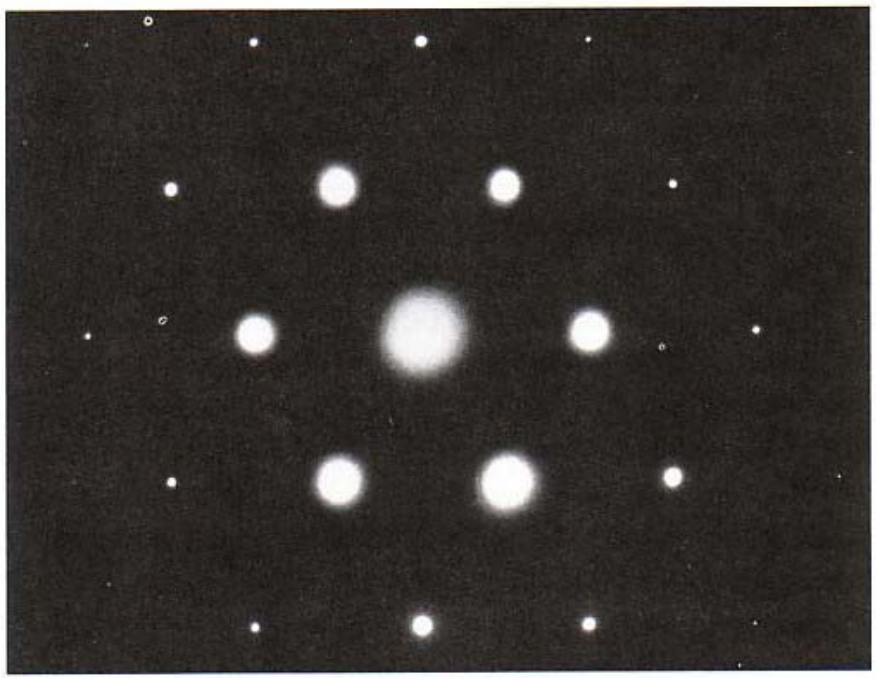

Figure 20.2. (A) SAD pattern from [111] Si showing the first few orders of diffraction spots but no Kikuchi lines. (B) CBED pattern from [111] Si showing dynamical contrast within the disks as well as Kikuchi and other lines.

Silicio

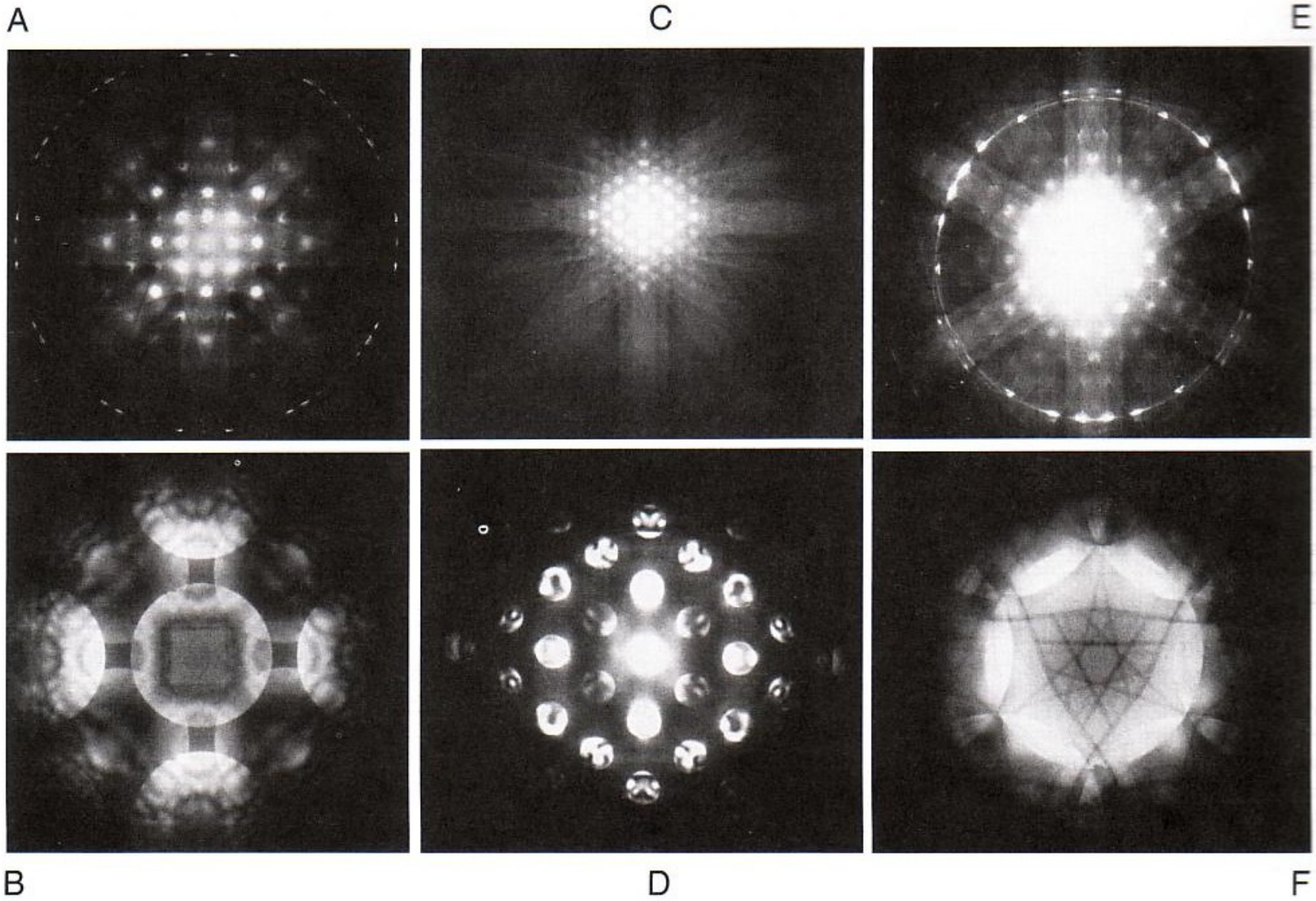

Figure 21.8. (A, B) [100], (C, D) [110], and (E, F) [111] ZAPs from stainless steel used to determine the point group. In (A, C, E) the low-*L* pattern gives the WP symmetry and in (B, D, F) the high-*L* pattern shows the BF symmetry. From the WP and BF symmetries, possible diffraction groups and point groups are determined, as summarized in Table 21.5.

Acero Inoxidable

Espesor de la muestra

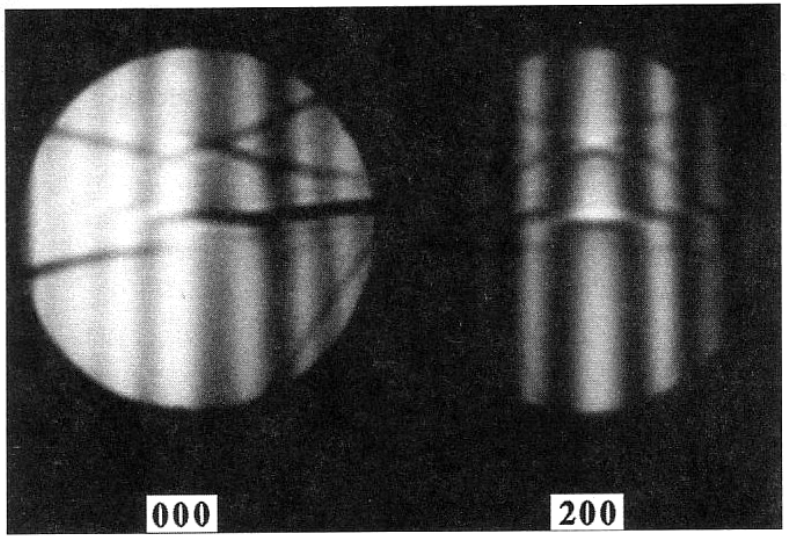

Figure 21.1. Kossel–Möllenstedt fringes in a ZOLZ CBED pattern from pure Al taken under two-beam conditions with (200) strongly excited.

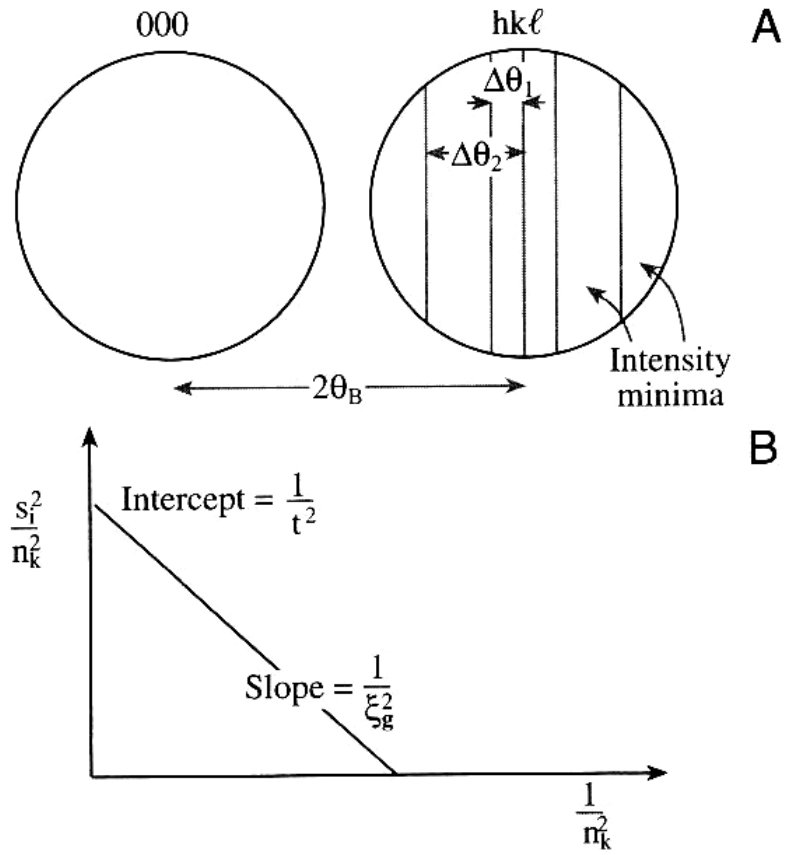

Figure 21.3. (A) The measurements necessary to extract thickness (t) from K–M fringes. From n_i measure spacings of $\Delta\theta_i$, determine the deviation parameters s_i, then (B) plot $(s_i/n_k)^2$ against n_k^2. If the plot is a straight line, extrapolate to the ordinate to find t^{-2}) and hence t.